Mechanics of Advanced Composite Structures

Semnan University

Journal homepage: https://macs.semnan.ac.ir/

ISSN:2423-7043

Research Article

Thick Sandwich Panel with Magnetorheological Core: Free Vibrations Analysis utilizing a novel sinusoidal shear deformation theory

Mehdi Keshavarzian[a*], Mohamad Ali Kazemi [b], Mostafa Kolivand [c]

[a] *Department of Mechanical Engineering, Technical and Vocational University (TVU), Tehran, Iran*
[b] *Department of Mechanical Engineering, Technical and Vocational University (TVU), Tehran, Iran*
[c] *Department of Mechanical Engineering, Technical and Vocational University (TVU), Tehran, Iran*

ARTICLE INFO

Article history:

Received: 2024-10-19
Revised: 2025-03-22
Accepted: 2025-05-12

Keywords:

Magnetorheological core;
Sinusoidal shear deformation theory;
Laminated composite face sheets;
Natural frequency;
Modal loss factor.

ABSTRACT

This study presents a free-vibration analysis of thick sandwich panels featuring a magnetorheological (MR) fluid core and elastic face sheets. The MR core exhibits field-dependent stiffness and damping characteristics, which are modeled to capture the rheological changes induced by external magnetic fields. A sinusoidal shear deformation theory is employed to formulate the structural response, eliminating the need for shear correction factors while accurately accounting for transverse shear deformation and rotary inertia. By applying Hamilton's principle, a set of fully coupled governing equations and associated boundary conditions are derived. The resulting complex eigenvalue problem is solved to determine the natural frequencies and modal loss factors of the adaptive structure. The influence of key geometric and material parameters—including magnetic field intensity, core thickness ratio, and panel aspect ratio—on the dynamic characteristics is investigated. The results demonstrate that increasing the magnetic field strength and aspect ratio leads to higher natural frequencies, whereas an increase in the core-to-panel thickness ratio reduces them. This analysis provides a comprehensive framework for predicting the vibrational behavior of MR-core sandwich panels under varying operational conditions.

1. Introduction

The development of high-order sandwich panel theories has significantly advanced the understanding of free vibration in panels with flexible cores.[1] Previous studies have explored various computational models to capture core behavior. For instance, early models considered vertical shear stresses in the core alongside face sheet displacements, while others, such as the Frostig model[2], utilized polynomial descriptions of core displacement fields based on these stresses. Further improvements to higher-order theories were introduced by Malekzadeh et al.[3], who applied first-order shear deformation theory to panels with viscoelastic cores. Recently, novel theoretical frameworks have been proposed to reduce the complexity of governing equations. For example, Guerine et al. formulated

* **Corresponding author.**
E-mail address: mkeshavarzian@tvu.ac.ir ,ORCID: 0000-0003-3660-4693

a new integral shear deformation shell theory for carbon nanotube-reinforced structures, which significantly reduces the number of independent variables compared to existing theories, ensuring traction-free boundary conditions without shear correction factors by using non-polynomial hyperbolic warping functions[4].

The integration of smart materials into sandwich structures has opened new avenues for adaptive vibration control. Nayak et al.[5] demonstrated a 30% vibration attenuation in cantilever sandwich beams using smart elastomers. More recently, Magnetorheological (MR) fluids and elastomers have attracted considerable attention due to their ability to change stiffness and damping properties under magnetic fields [6]. These adaptive structures offer enhanced vibration suppression across wide frequency ranges by exploiting rheological changes induced by external stimuli [7]. MR fluids consist of micron-sized iron particles suspended in a carrier fluid; under a high magnetic field, these particles form chain-like structures, resulting in a yield stress that is largely independent of particle size, although coarser particles can generate higher dynamic stress[8] . Slimani et al. also investigated the free vibration of functionally graded sandwich shells using a simple shear deformation theory, highlighting the sensitivity of fundamental frequencies to material distribution and geometric configurations[9].

Recent research has further expanded the application of advanced numerical methods in structural engineering. Rajamohan et al. [10] investigated the shear effects of MR binding layers on core behavior, while Lara-Prieto et al. [11]experimentally studied the controllability of vibrational properties in MR cantilever beams under varied magnetic intensities. Comparative studies between electrorheological (ER) and magnetorheological (MR) cores have also been conducted using higher-order shear deformation theories [12]. In the realm of finite element analysis, significant advancements have been made to address shear-locking issues. Belabed et al. introduced an enriched quadrilateral plate element with a discrete shear projection technique, which accelerates modal convergence and avoids shear-locking in graphene-reinforced plates [13]. Similarly, Widyatmoko et al. proposed a new four-node shell element (BKWH24) valid for thin to thick shells, incorporating membrane, bending, and transverse shear effects explicitly [14]. These numerical frameworks provide robust tools for predicting the dynamic behavior of complex composite structures.

Manoharan et al. [15]analyzed laminated composite MR plates, focusing on the influence of MR layer thickness and ply orientation. Other researchers, such as Jia-Yi Yeh [16]and Payganeh et al. [17] have explored MR elastomer damping and exponential shear deformation theories, respectively. Static analyses using sinusoidal shear deformation theory have also been proposed for functionally graded plates [18]. Despite these advancements, a significant research gap remains. Most existing studies rely on classical or first-order shear deformation theories, which may not accurately capture the complex shear deformation in thick sandwich panels with MR cores. Furthermore, while sinusoidal shear deformation theory has been successfully applied to static bending analyses of functionally graded plates[18], its application to the free-vibration analysis of MR-core sandwich panels—particularly considering the field-dependent stiffness and damping—has not been thoroughly investigated. This limitation highlights the need for a more robust theoretical framework that can accurately model the dynamic interaction between the magnetic field and the structural response, bridging the gap between advanced shell theories like those proposed by Guerine et al.[4] and the specific adaptive characteristics of MR materials.

The structural analysis of functionally graded (FG) and composite structures has undergone significant evolution, moving towards more complex geometries and material compositions. Early studies, such as the work by Rezaiee-Pajand et al. [19]established fundamental frameworks for the stability and vibration of tapered FG-sandwich columns with flexible connections. These concepts were subsequently extended to two-dimensional elements, where Rezaiee-Pajand et al. [20] developed robust formulations for the nonlinear analysis of FG-sandwich plates and shells. More recently, the scope of research has broadened to include advanced hybrid nanocomposites. For instance, Ghandehari et al. [21]investigated the multiscale dynamic behavior of nested conical shells reinforced with graphene nanoplatelets (GNPs) and carbon nanotubes (CNTs), highlighting the critical influence of nanofiller distribution and elastic interlayers on the system's natural frequencies. Building upon these progressive developments, the present study introduces a mixed interpolated formulation specifically designed to enhance the nonlinear analysis of FG-sandwich plates and shells while addressing numerical challenges like shear and membrane locking.

Beyond classical and analytical modeling, recent research has highlighted the significant advantages of data-driven methodologies in characterizing complex engineering systems. Intelligent optimization and machine learning, particularly Fully Connected Neural Networks (FCNNs) and Long Short-Term Memory (LSTM) networks, have been successfully applied to eliminate the need for cumbersome mathematical formulations in performance-based frameworks [22]. Such approaches offer superior scalability and lower computational costs for real-time parameter estimation and system identification. While the present study focuses on the rigorous mathematical verification of the equations of motion, integrating these intelligent predictive models represents a promising frontier for optimizing material properties and vibration responses in MR-related structures."

The primary motivation of this study is to fill this gap by employing a sinusoidal shear deformation theory to model the dynamic behavior of thick sandwich panels with MR cores. Unlike previous works that often decouple magnetic field effects from structural dynamics or rely on lower-order theories, this research explicitly accounts for the interaction between magnetic field intensity, geometric aspect ratio, and MR core thickness within a higher-order framework. The novelty of this work lies in the accurate prediction of natural frequencies and modal loss factors using the Navier solution method, providing a comprehensive tool for the design of adaptive vibration-damping systems. The rest of the paper is organized as follows: Section 2 presents the theoretical formulation, Section 3 presents the equations of motion, and Section 4 presents the results and Discussion.

2. Theoretical formulation and kinematic assumptions

The novel sinusoidal shear deformation theory of sandwich panels has been used to derive the governing equations of the problem. For both the face sheets and the core, the displacement field is based on the second Frostig model, to which the sinusoidal shear deformation theory has been applied. The displacements of the face sheets and core are assumed to be fully dynamic, and the unknowns are constant polynomial coefficients. Consider a thick composite sandwich panel composed of two composite laminated face sheets and an MR core layer. The thickness of the top face sheet, bottom face sheet, and core is h_t, h_b, h_c, respectively. The sandwich panel is supposed to have length a, width b, and total thickness h, as shown in Figure 1. It is also shown in Figure 1 where t and b refer to the top and bottom face sheets of the panel, respectively.

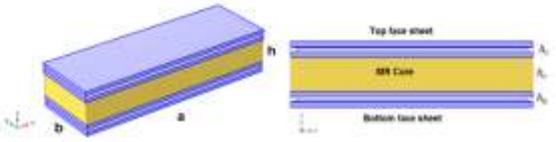

Fig.1. Sandwich plate with laminated composite sheets on the surfaces

2.1. Theoretical Formulation

Using new sinusoidal shear deformation, the small linear displacements of u, v, and w of the face sheets along the x, y (longitudinal), and z (thickness) axes are expressed by the following formulae.

$$u_i(x,z,y,t) = u_0^i(x,y,t) + f_1(z_i)\frac{\partial w_0(x,y,t)}{\partial x} + f_2(z_i)\phi_x^i(x,y,t)$$

$$v_i(x,z,y,t) = v_0^i(x,y,t) + f_1(z_i)\frac{\partial w_0(x,y,t)}{\partial y} + f_2(z_i)\phi_y^i(x,y,t) \; ; \; (i=t,b) \quad (1)$$

$$w_i(x,z,y,t) = w_0^i(x,y,t)$$

Where:

u_0^i, v_0^i, w_0^i : Displacement components of the face sheets

$$\phi_x^i(x,y,t) = \left(\frac{\partial \theta^i(x,y,t)}{\partial x} + \frac{\partial w_0^i(x,y,t)}{\partial x}\right)$$

$$\phi_y^i(x,y,t) = \left(\frac{\partial \theta^i(x,y,t)}{\partial y} + \frac{\partial w_0^i(x,y,t)}{\partial y}\right)$$

ϕ_x^i, ϕ_y^i : Rotation of the normal section of the mid surface of the top face sheet and bottom face sheet along x and y, respectively(i=t,b)

By introducing two unknown derivative quantities $\frac{\partial \theta(x,y,t)}{\partial x}$ and $\frac{\partial \theta(x,y,t)}{\partial y}$ the proposed sinusoidal shear deformation theory for each face sheet consists of only four unknown displacement functions — fewer than the five to eight unknowns required by other HSDTs, resulting in reduced computational cost. When combined with the five independent unknowns of the MR core $(u_{0c}, u_{1c}, v_{0c}, v_{1c}, w_{0c})$, obtained after applying the displacement compatibility conditions at the core–face sheet interfaces, the complete sandwich panel system yields a total of 13 coupled governing equations in 13 unknowns. The number of unknowns of the proposed theory is smaller than other HSDTs with five to eight unknowns, so the computation cost can be reduced. [23]. In this study, a novel sinusoidal shear deformation theory is obtained by setting the following:

$$f_1(z_i) = z_i \;,\; f_2(z_i) = \frac{h\sqrt{15}}{3\pi} sin\left(\frac{\pi z}{h}\right) \quad (2)$$

Thickness of the top face sheet, bottom face sheet, and core is h_t, h_b and h_c, respectively. The sandwich panel is supposed to have length a, width b, and total thickness h. The sinusoidal shear strain extraction function $f_2(z_i)$ is adopted to account for the non-linear distribution of transverse shear stresses through the thickness of the face-sheets. Unlike the classical plate theory, this function eliminates the need for a shear correction factor and ensures zero shear stress conditions at the top and bottom surfaces of the face-sheets.

The innovative sinusoidal shear deformation theory satisfies two requirements of the shear strains and stresses of the plates. The shear stress distribution must be parabolic over the plate thickness as the first condition. The second requirement is that the shear stresses and strains must be zero at all points on the two free surfaces of the plates. Consequently, the suggested theory does not need any shear correction parameters, unlike FSDTs where z_i is the vertical coordinate of each face sheet (i = t, b), measured upward from the mid-plane of each face sheet.

2.2. The theory used in the core

In this study, the core layer of the sandwich structure is modeled using Frostig's second model (Extended High-order Sandwich Panel Theory - EHSAPT) to accurately capture the transverse flexibility of the core. This model is characterized by the following fundamental assumptions:

1. The face sheets are modeled based on the First-order Shear Deformation Theory (FSDT), while the core is treated as a 3D elastic medium with nonlinear displacement fields.

2. The transverse normal stress of the core is assumed to vary through its thickness, allowing for the compressibility of the core (non-rigid core in the vertical direction).

3. Perfect bonding is assumed at the interfaces between the face sheets and the core.[2]

The displacement field of the middle core is considered to be a polynomial with unknown coefficients in accordance with the relations stated for the nucleus displacements in Frostig and Thomson's second model:

$$u_c(x,y,z,t) = u_0^c(x,y,t) + z_c u_1^c(x,y,t) + z_c^2 u_2^c(x,y,t) + z_c^3 u_3^c(x,y,t)$$

$$v_c(x,y,z,t) = v_0^c(x,y,t) + z_c v_1^c(x,y,t) + z_c^2 v_2^c(x,y,t) + z_c^3 v_3^c(x,y,t) \qquad (3)$$

$$w_c(x,y,z,t) = w_0^c(x,y,t) + z_c w_1^c(x,y,t) + z_c^2 w_2^c(x,y,t)$$

where: u_c, v_c, w_c :Displacement components of the core.

The polynomial coefficients u_c, v_c, w_c in the core displacement field are determined by invoking the displacement continuity conditions at the interfaces between the core and the face sheets ($z_{ct} = \frac{h_c}{2}$, $z_{cb} = -\frac{h_c}{2}$). By enforcing that the core displacements match the face-sheet displacements at these boundaries, the coefficients are explicitly expressed in terms of the primary kinematic variables of the top and bottom face sheets.

2.3. Definition of strain and displacement relationships for face sheets and cores

2.3.1. Define strain and displacement relationships for face sheets.

The strain and displacement field for the face sheets can be written as follows:[24]

$$\varepsilon_{xx}^i = \varepsilon_{0xx}^i + f_1(z_i)L_{xx}^i + f_2(z_i)k_{xx}^i$$

$$\varepsilon_{yy}^i = \varepsilon_{0yy}^i + f_1(z_i)L_{yy}^i + f_2(z_i)k_{yy}^i$$

$$\varepsilon_{zz}^i = 0$$

$$\gamma_{xy}^i = 2\varepsilon_{xy}^i = \gamma_{0xy}^i + f_1(z_i)L_{xy}^i + f_2(z_i)k_{xy}^i$$

$$\gamma_{xz}^i = 2\varepsilon_{xz}^i = \gamma_{0xz}^i + \frac{\partial f_1(z_i)}{\partial z_i}G_{xz}^i + \frac{\partial f_2(z_i)}{\partial z_i}T_{xz}^i, \qquad (4)$$

$$\gamma_{yz}^i = 2\varepsilon_{yz}^i = \gamma_{0yz}^i + \frac{\partial f_1(z_i)}{\partial z_i}G_{yz}^i + \frac{\partial f_2(z_i)}{\partial z_i}T_{yz}^i$$

$$\varepsilon_{0xx}^i = \frac{\partial u_0^i}{\partial x},\quad \varepsilon_{0yy}^i = \frac{\partial v_0^i}{\partial y},\ \gamma_{0xy}^i = \frac{\partial v_0^i}{\partial x} + \frac{\partial u_0^i}{\partial y}$$
$$\gamma_{0xz}^i = \frac{\partial w_0^i}{\partial x},\ \gamma_{0yz}^i = \frac{\partial w_0^i}{\partial y},\ L_{xx}^i = \frac{\partial^2 w_0^i}{\partial x^2},$$
$$k_{xx}^i = \frac{\partial \phi_x^i}{\partial x},\quad L_{yy}^i = \frac{\partial^2 w_0^i}{\partial y^2},\quad k_{yy}^i = \frac{\partial \phi_y^i}{\partial y}, \qquad (5)$$
$$L_{xy}^i = 2\frac{\partial^2 w_0^i}{\partial x \partial y},\quad k_{xy}^i = \frac{\partial \phi_x^i}{\partial y} + \frac{\partial \phi_y^i}{\partial x},$$
$$G_{xz}^i = \frac{\partial w_0^i}{\partial x},\ T_{xz}^i = \phi_x^i,\ G_{yz}^i = \frac{\partial w_0^i}{\partial y},\ T_{yz}^i = \phi_y^i$$

2.3.2. Define strain and displacement relationships for core

$$\varepsilon_{xx}^c = \frac{\partial u_c}{\partial x},\ \varepsilon_{yy}^c = \frac{\partial v_c}{\partial y},\ \varepsilon_{zz}^c = \frac{\partial w_c}{\partial z}$$
$$\gamma_{xy}^c = 2\varepsilon_{xy}^c = \frac{\partial v_c}{\partial x} + \frac{\partial u_c}{\partial y},\ \gamma_{xz}^c = 2\varepsilon_{xz}^c = \frac{\partial w_c}{\partial x} + \frac{\partial u_c}{\partial z} \qquad (6)$$
$$\gamma_{yz}^c = 2\varepsilon_{yz}^c = \frac{\partial w_c}{\partial y} + \frac{\partial v_c}{\partial z}$$

To use viscoelastic materials such as electrorheological and magnetorheological in the core, we assume that we are in the condition before yielding and the material is modeled as linear viscoelastic. By inserting the expressions related to the displacement field of the nucleus, the relations (1) in the relations (6) of the strains in terms of displacement of the middle surface can be obtained as follows:[3]

$$\varepsilon_{xx}^c = (\varepsilon_{0xx} + z_c\chi_{0xx} + z_c^2\varepsilon_{0xx}^* + z_c^3\chi_{0xx}^*),$$
$$\varepsilon_{yy}^c = (\varepsilon_{0yy} + z_c\chi_{0yy} + z_c^2\varepsilon_{0yy}^* + z_c^3\chi_{0yy}^*)$$
$$\varepsilon_{zz}^c = \varepsilon_{0zz} + z_c\chi_{0zz}$$

$$\gamma_{xy}^{c} = \varepsilon_{0xy} + z_c\chi_{0xy} + {z_c}^2\varepsilon_{0xy}^{*} + {z_c}^3\chi_{0xy}^{*} + \varepsilon_{0yx} + z_c\chi_{0yx} + {z_c}^2\varepsilon_{0yx}^{*} + {z_c}^3\chi_{0yx}^{*} \quad (7)$$

$$\gamma_{xz}^{c} = \varepsilon_{0xz} + z_c\chi_{0xz} + {z_c}^2\varepsilon_{0xz}^{*} + {z_c}^3\chi_{0xz}^{*} + \varepsilon_{1xz} + z_c\chi_{1xz} + {z_c}^2\varepsilon_{1xz}^{*}$$

$$\gamma_{yz}^{c} = \varepsilon_{0yz} + z_c\chi_{0yz} + {z_c}^2\varepsilon_{0yz}^{*} + {z_c}^3\chi_{0yz}^{*} + \varepsilon_{1yz} + z_c\chi_{1yz} + {z_c}^2\varepsilon_{1yz}^{*}$$

$$\varepsilon_{0xx} = \frac{\partial u_0^c}{\partial x}, \quad \chi_{0xx} = \frac{\partial u_1^c}{\partial x} \quad , \varepsilon_{0xx}^{*} = \frac{\partial u_2^c}{\partial x}$$
$$\chi_{0xx}^{*} = \frac{\partial u_3^c}{\partial x}, \varepsilon_{0yy} = \frac{\partial v_0^c}{\partial y},$$

$$\chi_{0yy} = \frac{\partial v_1^c}{\partial y}, \varepsilon_{0yy}^{*} = \frac{\partial v_2^c}{\partial y}, \quad \chi_{0yy}^{*} = \frac{\partial v_3^c}{\partial y}, \varepsilon_{0zz} = w_1^c,$$
$$\chi_{0zz} = 2w_2^c$$

$$\varepsilon_{0xy} = \frac{\partial v_0^c}{\partial x}, \chi_{0xy} = \frac{\partial v_1^c}{\partial x}, \quad \varepsilon_{0xy}^{*} = \frac{\partial v_2^c}{\partial x},$$

$$\chi_{0xy}^{*} = \frac{\partial v_3^c}{\partial x}, \varepsilon_{0yx} = \frac{\partial u_0^c}{\partial y}, \quad \chi_{0yx} = \frac{\partial u_1^c}{\partial y} \quad (8)$$
$$\varepsilon_{0yx}^{*} = \frac{\partial u_2^c}{\partial y}, \quad \chi_{0yx}^{*} = \frac{\partial u_3^c}{\partial y},$$
$$\varepsilon_{0xz} = \frac{\partial w_0^c}{\partial x}, \chi_{0xz} = \frac{\partial w_1^c}{\partial x}, \quad \varepsilon_{0xz}^{*} = \frac{\partial w_2^c}{\partial x}, \chi_{0xz}^{*} = 0$$

$$\varepsilon_{1xz} = u_1^c, \quad \chi_{1xz} = 2u_2^c, \quad \varepsilon_{xz}^{*} = 3u_3^c$$
$$\varepsilon_{0yz} = \frac{\partial w_0^c}{\partial y}, \quad \chi_{0yz} = \frac{\partial w_1^c}{\partial y}, \quad \varepsilon_{0yz}^{*} = \frac{\partial w_2^c}{\partial y}$$

$$\chi_{0xy}^{*} = 0, \quad \varepsilon_{1yz} = v_1^c, \chi_{1yz} = 2v_2^c, \varepsilon_{yz}^{*} = 3v_3^c$$

2.3.3. Compatibility conditions

The strain functions are considered to be continuous at the connecting surfaces of the layers. The layers, and the middle core are all assumed to be entirely bound together. As a result, the following compatibility requirements will apply at the location where the core is attached to the face sheets.

The interface coordinates are defined at the junctions of the core and face sheets. Let $z_{ct} = \frac{h_c}{2}$ denote the top interface and $, z_{cb} = -\frac{h_c}{2}$ denote the bottom interface. The parameter k is an indicator used to maintain the correct sign for the relative distances from the mid-plane of each face sheet to the respective interface.[3]

$$\begin{cases} u_c(z = z_{ci}) = u_0^i + \frac{1}{2}(-1)^k h_i \phi_x^i \\ v_c(z = z_{ci}) = v_0^i + \frac{1}{2}(-1)^k h_i \phi_y^i \\ w_c(z = z_{ci}) = w_0^i \end{cases}$$

$$\begin{cases} For\ i = t \rightarrow \left(k = 1 ؛ z_{ct} = \frac{h_c}{2}\right) \\ For\ i = b \rightarrow \left(k = 0 ؛ z_{cb} = -\frac{h_c}{2}\right) \end{cases} \quad (9)$$

The number of unknowns and equations is reduced by placing the relations of displacement fields of face sheets (1) and core (3) in relations (9), and obtaining relations between dependent coefficients. Therefore, the 11 unknown parameters of the core are reduced to 5 independent unknowns, namely $u_0^c, u_1^c, v_0^c, v_1^c, w_0^c$

2.3.4. Stress resultants for the core layer

Stress resultants per unit length for the core layer are defined as demonstrated below:

$$\begin{Bmatrix} N_{xx}^c \\ N_{yy}^c \\ N_{xy}^c \end{Bmatrix} = \int_{-h_c/2}^{h_c/2} \begin{Bmatrix} \sigma_{xx}^c \\ \sigma_{yy}^c \\ \sigma_{xy}^c \end{Bmatrix} dz_c, \begin{Bmatrix} M_{nxx}^c \\ M_{nyy}^c \\ M_{nxy}^c \end{Bmatrix} =$$
$$\int_{-h_c/2}^{h_c/2} z_c^n \begin{Bmatrix} \sigma_{xx}^c \\ \sigma_{yy}^c \\ \sigma_{xy}^c \end{Bmatrix} dz_c, \begin{Bmatrix} N_{xz}^c \\ N_{yz}^c \\ M_{nxz}^c \\ M_{nyz}^c \end{Bmatrix} =$$
$$\int_{-h_c/2}^{h_c/2} z_c^n \begin{Bmatrix} \sigma_{xz}^c \\ \sigma_{yz}^c \\ z_c^n \sigma_{xz}^c \\ z_c^n \sigma_{yz}^c \end{Bmatrix} dz_c \quad (10)$$
$$\{R_z^c, M_z^c\} = \int_{-h_c/2}^{h_c/2} (1, z_c)\sigma_{zz}^c dz_c, n = 1,2,3$$

2.3.5. Stress resultants for the face sheets

Stress resultants per unit length for the face sheets can be defined as follows:[3]

$$\begin{Bmatrix} N_{xx}^i \\ N_{yy}^i \\ N_{xy}^i \end{Bmatrix} = \int_{-h_i/2}^{h_i/2} \begin{Bmatrix} \sigma_{xx}^i \\ \sigma_{yy}^i \\ \sigma_{xy}^i \end{Bmatrix} dz_i,$$
$$\begin{Bmatrix} M_{xx}^i \\ M_{yy}^i \\ M_{xy}^i \end{Bmatrix} = \int_{-h_i/2}^{h_i/2} f_1(z_i) \begin{Bmatrix} \sigma_{xx}^i \\ \sigma_{yy}^i \\ \sigma_{xy}^i \end{Bmatrix} dz_i,$$
$$\begin{Bmatrix} P_{xx}^i \\ P_{yy}^i \\ P_{xy}^i \end{Bmatrix} = \int_{-h_i/2}^{h_i/2} f_2(z_i) \begin{Bmatrix} \sigma_{xx}^i \\ \sigma_{yy}^i \\ \sigma_{xy}^i \end{Bmatrix} dz_i$$

$$N_{xz}^i = \int_{-h_i/2}^{h_i/2} \sigma_{xz}^i dz_i,$$
$$R_{xz}^i = \int_{-h_i/2}^{h_i/2} \left(\frac{\partial f_1(z_i)}{\partial z}\right) \sigma_{xz}^i dz_i,$$
$$S_{xz}^i = \int_{-h_i/2}^{h_i/2} \left(\frac{\partial f_2(z_i)}{\partial z}\right) \sigma_{xz}^i dz_i, \ (i = t, b) \quad (11)$$

$$N_{yz}^i = \int_{-h_i/2}^{h_i/2} \sigma_{yz}^i dz_i,$$
$$R_{yz}^i = \int_{-h_i/2}^{h_i/2} \left(\frac{\partial f_1(z_i)}{\partial z}\right) \sigma_{yz}^i dz_i,$$
$$S_{yz}^i = \int_{-h_i/2}^{h_i/2} \left(\frac{\partial f_2(z_i)}{\partial z}\right) \sigma_{yz}^i dz_i,$$

To provide a systematic derivation of the governing equations, the following procedure is adopted: First, the displacement fields for the face sheets and the core are defined based on the kinematic assumptions (Eqs.1-8). By applying the compatibility conditions (Eq. 9), the core coefficients are linked to the primary variables. Then, the strain-displacement relations (Eqs.7-8) are derived, which are subsequently used in the constitutive equations to obtain the stress components. Finally, by employing Hamilton's Principle, the energy terms are integrated to formulate the governing vibration equations in terms of stress resultants.

3. Equations of motion

Hamilton's principle is used to derive the motion equations of the sandwich panel and to perform dynamic analysis. The analytical form of Hamilton's principle can be expressed as follows:

$$\int_{t_1}^{t_2} \delta L dt = \int_{t_1}^{t_2} (\delta K - \delta U + \delta W_{ext}) dt = 0 \quad (12)$$

where δK represents changes in kinetic energy, δU represents changes in potential energy, and δW_{ext} represents changes in energy caused by external forces. Here, because the aim is to check free vibrations, this value is equal to zero (δW_{ext}=0).

3.1. Kinetic energy

By applying Hamilton's principle and performing integration by parts with respect to time, and considering that the variations of displacements are zero at t_1 and t_2, the virtual kinetic energy of the system δK can be expressed in terms of acceleration components as follows:

$$\delta K = -\sum_{i=t,b,c}\left[\iint_{A_i}\int_{-h_i/2}^{h_i/2} \rho_i(\ddot{u}_i\delta u_i + \ddot{v}_i\delta v_i + \ddot{w}_i\delta w_i)dz_i\, dA_i\right] \quad (13)$$

$$dA_c = dx_c dy_c, \quad dA_i = dx_i dy_i, \quad (i = t, b)$$

3.2. Strain energy

The total strain energy stored in the tops and core of the sandwich panel is expressed by the following relationship:

$$\delta U = \sum_{i=t,b}\left(\int_{V_i}(\sigma^i_{xx}\delta\varepsilon^i_{xx} + \sigma^i_{yy}\delta\varepsilon^i_{yy} + \tau^i_{xy}\delta\gamma^i_{xy} + \tau^i_{xz}\delta\gamma^i_{xz} + \tau^i_{yz}\delta\gamma^i_{yz})dV_i\right) + \int_{V_c}(\tau^c_{xy}\delta\gamma^c_{xy} + \tau^c_{xz}\delta\gamma^c_{xz} + \tau^c_{yz}\delta\gamma^c_{yz})dV_c \quad (14)$$

$dV_c = dA_c dz_c = dx_c dy_c dz_c$, $dV_i = dA_i dz_i = dx_i dy_i dz_i$; $(i = t, b)$

Finally, by replacing the relations of stresses, resulting stresses (10-11), as well as replacing the relations related to displacement fields (1-2) and strain-displacement relations (5-6) in the relations of changes in kinetic energy and potential System (13-14) and using Hamilton's principle (12) and the basic principle of calculus of variations, the linear equations of motion for a sandwich plate with a flexible core are obtained as a series of partial differential equations with 13 equations and 13 unknowns. For example:

δw_0^C:

$$\frac{\partial N^C_{xz}}{\partial x} - \frac{4}{h_c^2}\frac{\partial M^C_{2xz}}{\partial x} - \frac{4}{h_c^2}\frac{\partial M^C_{2yz}}{\partial y} + \frac{\partial N^C_{yz}}{\partial y} + \frac{8}{h_c^2}M^C_z = \left(\frac{16I_4^C}{h_c^4} - \frac{8I_2^C}{h_c^2} + I_0^C\right)\ddot{w}_0^C + \left(\frac{2I_2^C}{h_c^2} - \frac{8I_4^C}{h_c^4} + \frac{I_1^C}{h_c} - \frac{4I_3^C}{h_c^3}\right)\ddot{w}_0^t + \left(\frac{2I_2^C}{h_c^2} - \frac{8I_4^C}{h_c^4} - \frac{I_1^C}{h_c} + \frac{4I_3^C}{h_c^3}\right)\ddot{w}_0^b \quad (15)$$

3.3. Moments of inertia for the face sheets and core layer

Moments of inertia of the face sheets are defined as demonstrated below:

$$I_0^t = \int_{-\frac{h_t}{2}}^{\frac{h_t}{2}} \rho_t\, dz_t$$

$$I_1^t = \int_{-\frac{h_t}{2}}^{\frac{h_t}{2}} \rho_t\, f_1(z_i) dz_t$$

$$I_2^t = \int_{-\frac{h_t}{2}}^{\frac{h_t}{2}} \rho_t\, f_2(z_i) dz_t$$

$$I_3^t = \int_{-\frac{h_t}{2}}^{\frac{h_t}{2}} \rho_t\, f_1(z_i) f_2(z_i) dz_t$$

$$I_4^t = \int_{-\frac{h_t}{2}}^{\frac{h_t}{2}} \rho_t\, [f_2(z_i)]^2 dz_t$$

$$I_0^b = \int_{-\frac{h_b}{2}}^{\frac{h_b}{2}} \rho_b\, dz_b$$

$$I_1^b = \int_{-\frac{h_b}{2}}^{\frac{h_b}{2}} \rho_b\, f_1(z_i) dz_b \quad (16)$$

$$I_2^b = \int_{-\frac{h_b}{2}}^{\frac{h_b}{2}} \rho_b\, f_2(z_i) dz_b$$

$$I_3^b = \int_{-\frac{h_b}{2}}^{\frac{h_b}{2}} \rho_b\, f_1(z_i) f_2(z_i) dz_b$$

$$I_4^b = \int_{-\frac{h_b}{2}}^{\frac{h_b}{2}} \rho_b\, [f_2(z_i)]^2 dz_b$$

Moments of inertia for the core layer as indicated below:

$$I_n^c = \int_{-\frac{h_c}{2}}^{\frac{h_c}{2}} \rho_c z_c^n \, dz_c \qquad n = 0,1,\dots,6 \qquad (17)$$

3.4 Lamina constitutive Relations

The linear constitutive relations for the k[th] orthotropic lamina in the principal material coordinates of a lamina are :[24]

$$\begin{bmatrix}\sigma_{xx}\\ \sigma_{yy}\\ \sigma_{xy}\end{bmatrix} = \begin{bmatrix}Q_{11} & Q_{12} & Q_{16}\\ Q_{12} & Q_{22} & Q_{26}\\ Q_{16} & Q_{26} & Q_{66}\end{bmatrix}^{(k)} \begin{bmatrix}\varepsilon_{xx}\\ \varepsilon_{yy}\\ \varepsilon_{xy}\end{bmatrix}$$

$$\begin{bmatrix}\sigma_{yz}\\ \sigma_{xz}\end{bmatrix} = \begin{bmatrix}Q_{44} & Q_{45}\\ Q_{45} & Q_{55}\end{bmatrix}^{(k)} \begin{bmatrix}\varepsilon_{yz}\\ \varepsilon_{xz}\end{bmatrix} \qquad (18)$$

Where $Q_{ij}^{(k)}$ are the plane stress-reduced stiffness. The coefficients are known in terms of the engineering constants of the kth layer:

$$Q_{11} = \frac{E_1}{1-\nu_{12}\nu_{21}}, Q_{12} = \frac{\nu_{12}E_1}{1-\nu_{12}\nu_{21}}, Q_{22} = \frac{E_2}{1-\nu_{12}\nu_{21}}, Q_{66} = G_{12}, Q_{44} = G_{23}, Q_{55} = G_{13} \qquad (19)$$

The constitutive equations of each layer must be transformed to the laminate coordinates because the laminate is composed of a number of orthotropic layers with material axes that can be oriented arbitrarily with respect to the laminate coordinates. The stress-strain relationships along the geometrical axes of the sandwich panel are as follows:[24]

$$\begin{bmatrix}\sigma_{xx}\\ \sigma_{yy}\\ \sigma_{xy}\end{bmatrix} = \begin{bmatrix}\bar{Q}_{11} & \bar{Q}_{12} & \bar{Q}_{16}\\ \bar{Q}_{12} & \bar{Q}_{22} & \bar{Q}_{26}\\ \bar{Q}_{16} & \bar{Q}_{26} & \bar{Q}_{66}\end{bmatrix}^{(k)} \begin{bmatrix}\varepsilon_{xx}\\ \varepsilon_{yy}\\ \varepsilon_{xy}\end{bmatrix}$$

$$\begin{bmatrix}\sigma_{yz}\\ \sigma_{xz}\end{bmatrix} = \begin{bmatrix}\bar{Q}_{44} & \bar{Q}_{45}\\ \bar{Q}_{45} & \bar{Q}_{55}\end{bmatrix} \begin{bmatrix}\varepsilon_{yz}\\ \varepsilon_{xz}\end{bmatrix} \qquad (20)$$

Where $\bar{Q}_{ij}$ denotes the transmitted stiffness in the geometric axis of the sandwich panel. The relationship between axial stiffness and the transferred stiffness is given by the relation:

$$\bar{Q}_{11} = Q_{11}cos^4\theta + 2(Q_{12} + 2Q_{66})sin^2\theta\, cos^2\theta + Q_{22}sin^4\theta$$

$$\bar{Q}_{12} = (Q_{11} + Q_{22} - 4Q_{66})sin^2\theta\, cos^2\theta + Q_{12}(sin^4\theta + cos^4\theta)$$

$$\bar{Q}_{22} = Q_{11}sin^4\theta + 2(Q_{12} + 2Q_{66})sin^2\theta\, cos^2\theta + Q_{22}cos^4\theta$$

$$\bar{Q}_{16} = (Q_{11} - Q_{12} - 2Q_{66})sin\theta\, cos^3\theta + (Q_{12} - Q_{22} + 2Q_{66})sin^3\theta\, cos\theta \qquad (21)$$

$$\bar{Q}_{26} = (Q_{11} - Q_{12} - 2Q_{66})sin^3\theta\, cos\theta + (Q_{12} - Q_{22} + 2Q_{66})sin\theta\, cos^3\theta$$

$$\bar{Q}_{66} = (Q_{11} + Q_{22} - 2Q_{12} - 2Q_{66})sin^2\theta cos^2\theta + Q_{66}(sin^4\theta + cos^4\theta)$$

$$\bar{Q}_{44} = Q_{44}cos^4\theta + Q_{55}sin^4\theta$$

$$\bar{Q}_{45} = (Q_{55} - Q_{44})\, cos\theta sin\,\theta$$

$$\bar{Q}_{55} = Q_{55}cos^4\theta + Q_{44}sin^4\theta$$

3.5. Model of MR material

It has been widely reported that the storage (G') and loss moduli (G'') of the MR fluids, prior to saturation, can be described by quadratic functions in the magnetic flux density field.[10, 25-27]. In the pre-yield regime, the MR material demonstrates viscoelastic behavior, which has been described in terms of the complex modulus:

$$G = G' + iG''$$

where G' is storage modulus of the MR fluid, which is related to the average energy stored per unit volume of the material during a deformation cycle, and G'' is the loss modulus, a measure of the energy dissipated per unit volume of the material over a cycle. The storage and loss moduli of the MR fluid were estimated corresponding to different magnetic field intensities (0, 100, 200, 300,450,500 and 600 Gauss). Both the storage and shear moduli were expressed using the following second-order polynomial functions with respect to the field intensity:[10]

$$G'(\beta) = -3.3691\beta^2 + 4.9975 \times 10^3\beta + 0.873 \times 10^6$$

$$G''(\beta) = -0.9\beta^2 + 0.8124 \times 10^3\beta + 0.1855 \times 10^6$$

$$G(\beta) = G'(\beta) + iG''(\beta)$$

Where β is the intensity of the magnetic field in Gauss. The quadratic relationship between the MR core properties and the magnetic field intensity is a widely accepted simplification in sandwich structure analysis. This model accurately captures the behavior of the MR fluid in the pre-saturation regime, which is the focus of the current vibration study.

Since the present study investigates small-strain free vibrations, the shear strain levels in the MR core remain significantly below the yield strain. Therefore, the linear viscoelastic (pre-yield) assumption is physically justified, and post-yield flow behavior does not occur during these oscillations.

In this work, the complex shear modulus is treated as frequency-independent within the investigated range to isolate the effects of the magnetic field. However, the proposed complex eigenvalue formulation is robust enough to incorporate frequency-dependent properties in future studies.

No normal stress exists in the MR layer, and there exist only transverse shear stresses as follows:

$$\sigma_{xz}^{c} = G(B)_{xz}^{c}\gamma_{xz}^{c} = G(B)_{xz}^{c}\left[\frac{\partial w_0^C}{\partial x} + z\frac{\partial w_1^C}{\partial x} + z^2\frac{\partial w_2^C}{\partial x}\right] + G(B)_{xz}^{c}[u_1^c + 2zu_2^c + 3z^2u_3^c] \qquad (22)$$

$$\sigma_{yz}^{c} = G(B)_{yz}^{c}\gamma_{yz}^{c} = \sigma_{yz}^{c}\left[\frac{\partial w_0^C}{\partial y} + z\frac{\partial w_1^C}{\partial y} + z^2\frac{\partial w_2^C}{\partial y}\right] + G(B)_{yz}^{c}[v_1^c + 2zv_2^c + 3z^2v_3^c] \qquad (23)$$

On all four edges of the sandwich plate in this analysis, simply supported boundary conditions are taken as given. It may be demonstrated that the relationship's assumed responses meet the simply supported boundary criteria.

$$\begin{bmatrix} u_0^j(x,y,t) \\ v_0^j(x,y,t) \\ w_0^j(x,y,t) \\ \theta^j(x,y,t) \\ u_k^c(x,y,t) \\ v_k^c(x,y,t) \\ w_0^c(x,y,t) \end{bmatrix} = \sum_{n=1}^{\infty}\sum_{m=1}^{\infty} \begin{bmatrix} U_{0mn}^j cos\,(\alpha_m x) sin(\beta_n y) \\ V_{0mn}^j sin\,(\alpha_m x) cos(\beta_n y) \\ W_{0mn}^j sin\,(\alpha_m x) sin(\beta_n y) \\ \theta_{0mn}^j sin\,(\alpha_m x) sin(\beta_n y) \\ U_{kmn}^c cos\,(\alpha_m x) sin(\beta_n y) \\ V_{kmn}^c sin\,(\alpha_m x) cos(\beta_n y) \\ W_{lmn}^j sin\,(\alpha_m x) sin(\beta_n y) \end{bmatrix} e^{i\omega t},$$

$$(k = 0,1,2,3), (l = 0,1,2) \qquad (24)$$

where $\alpha_m = \frac{m\pi}{a}$ *and* $\beta_n = \frac{n\pi}{b}$

In Equation (24) $W_{lmn}^j, V_{kmn}^c, U_{kmn}^c, \theta_{0mn}^j, W_{0mn}^j, U_{0mn}^j, V_{0mn}^j$ are the Fourier coefficients while m and n represent half-wave numbers along the x and y directions, respectively. By replacing equations (24) in the governing equations of motion, they are transformed to ordinary coupled differential equations:

$$[K - \lambda_{mn}M]\{c\} = \{0\} \qquad (25)$$

$$\{c\} = \{U_{0mn}^t, U_{0mn}^b, V_{0mn}^t, V_{0mn}^b, W_{0mn}^t, W_{0mn}^b, \theta_{0mn}^t, \theta_{0mn}^b, U_{0mn}^c, V_{0mn}^c, U_{1mn}^c, V_{1mn}^c, W_{0mn}^c\}^t$$

where, $\lambda_{mn} = \omega_{mn}^2$ and $\{c\}$ is the displacement vector for all the values of m and n. The stiffness and mass matrices are [K] and [M], respectively.

The eigenvalue parameter, λ_{mn} is a complex quantity due to the frequency-dependent complex shear modulus of the MR core. It is related to the complex natural frequency ω of the sandwich structure as $\lambda_{mn} = \omega_{mn}^2$. The real and imaginary parts of this complex eigenvalue are subsequently used to determine the natural frequencies and modal loss factors, as defined in Eq.(26). To determine the dynamic characteristics of the MR sandwich plate, the complex eigenvalue, denoted as $(\widetilde{\omega}^2)$, is analyzed. This complex parameter encapsulates both the elastic storage and viscous dissipation properties of the system. The real part of the complex eigenvalue, $\sqrt{Re(\widetilde{\omega}^2)}$, represents the square of the system's damped natural frequency, while the ratio of the imaginary part to the real part defines the modal loss factor η_v. The modal loss factor is a non-dimensional measure of the energy dissipated per radian to the peak strain energy stored in the system during a cycle of vibration. Accordingly, these parameters are extracted as follows:

$$\omega = \sqrt{Re(\widetilde{\omega}^2)}, \quad \eta_v = \frac{Im(\widetilde{\omega}^2)}{Re(\widetilde{\omega}^2)} \qquad (26)$$

Due to the complex-valued shear modulus of the MR core, the resulting global stiffness matrix [K] is complex and frequency-dependent. Consequently, the governing equations lead to a complex eigenvalue problem of the form

$[K - \lambda_{mn}M]\{c\} = \{0\}$. To solve this, an iterative procedure is employed, or a direct solver for complex matrices is used. The extraction of physical parameters is performed by decomposing the complex eigenvalue λ into its real and imaginary parts, as detailed in Eq. (26), to obtain the natural frequencies and modal loss factors, respectively.

4. Results and Discussion

4.1. Computational Implementation

The governing equations of motion and the resulting numerical formulations were verified and implemented using Wolfram Mathematica (version 12). The powerful symbolic computation engine of Mathematica was utilized to perform the rigorous derivation of the governing equations and to verify the mathematical consistency of the differential operators. For the numerical solution of the nonlinear problems and the extraction of critical values, the built-in high-precision numerical solvers of the software were employed. Additionally, for data post-processing, the generation of professional-grade figures, and the construction of detailed tables, Origin Pro software was used. All computational tools were utilized under academic licenses to ensure the accuracy and reproducibility of the presented results.

The linear vibrations of a rather thick sandwich panel with a smart magnetorheological core were examined in this article. The second Frostig model, which is based on the flexibility of the core, and the new sinusoidal theory for face sheets were used to get the equations of motion in terms of in-plane displacements. The equations of motion were verified using a mathematical program. It might be good to highlight the overall validity and accuracy of the work before giving the important numerical figures. Accordingly, we first computed the lowest natural frequency for each mode number for a three-layer rectangular sandwich plate with viscoelastic core using the Riley-Ritz method with its physical and geometrical parameters as given in of [28]. The numerical results, as shown in Table 1, show very good agreement with those displayed in Table 1. As a final check, the first four frequencies of the sandwich plates were compared with the results of [15] and [16]. In the investigated problem, the lay-up sequence was [0, core, 0], and all mechanical specifications were taken from reference [15]. In reference [15], there was an adhesive layer with a thickness of 1 mm between the layers. According to Table 2, there is a good agreement between the results of the present research and the results of references [15] and [16].

4.2. Free vibration of a simply-supported pane

In this section, the free vibrations of a sandwich panel with composite face sheets and MR core using a novel sinusoidal shear deformation theory have been investigated, and the effects of changing the thickness of the MR layer, aspect ratio, and magnetic field intensity on the natural frequencies and the modal loss factor of the panels have been investigated. The mechanical and geometric characteristics of the desired structure in this section are presented in Table 3. The sandwich panel is symmetric about the mid-plane, and the lay-up sequences for the face sheets are [0, 90, 0, core, 0, 90, 0]. The most important observations are as follows. The natural frequencies increase with increasing magnetic field strength. In particular, the effect of increasing magnetic field strength is more evident on the natural frequencies associated with the higher mode numbers in comparison with those of the lower modes.

To determine the vibration characteristics, a complex eigenvalue analysis is performed. The frequency-dependent properties of the MR core result in a complex stiffness matrix. The real part of the resulting eigenvalues provides the natural frequencies, while the modal loss factors are extracted from the ratio of the imaginary part to the real part of the eigenvalues, representing the system's damping capacity for each mode.

Table. 1. Comparison of natural frequencies obtained by Lall et al [28] and RK Ojha [29] with those obtained in the present methods.

	Lall et al [28]		RK Ojha [29]		Present		error analysis Lall et al & Present	error analysis RK Ojha & Present
Mode	Natural frequency (Hz)	Loss factor	Natural frequency (Hz)	Loss factor	Natural frequency (Hz)	Loss factor	Natural frequency (Hz)	Natural frequency (Hz)
1	155.20	0.04431	156.30	-	155.131	0.0438	۰/۰۴٪	۰/۶۳٪
2	374.14	0.01918	372.83	-	373. 67	0.01910	۰/۱۲٪	۰/۲۲٪
3	374.14	0.01918	377.63	-	373.67	0.01910	۰/۱۲٪	۱/۰۴٪
4	593.22	0.01224	593.97	-	591.71	0.01221	۰/۲۵٪	۰/۳۸٪

Table. 2. Comparison of natural frequency obtained by Manoharan et al [15] and Yeh[16] with those obtained in the present methods (G is the intensity of the magnetic field in gauss).

	Manoharan et al [15]	Yeh[16]	Present
	G=400 Gauss	G=400 Gauss	G=400 Gauss
Mode	Natural	Natural	Natural

	frequency (Hz)	Frequency (Hz)	frequency (Hz)
1	116.75	115.01	116.334
2	184.11	195.21	199.247
3	300.31	296.21	296.476
4	325.15	327.15	327.3

Table 3. Mechanical and geometrical properties of the composite sandwich panel with multi-layer face sheets and MR core.

Geometry	Laminate face sheets	MR Core
a=0.3m	ρ =1627 Kg/m3	ρ =3500 Kg/m3
b=0.3m	E_1=131 GPa E_2=E_3=10.34 GPa	$G_{12} = G_{13}$ =G_{23}= $G = G' + \mathrm{i}G''$
h_c = 1mm	$G_{12} = G_{23}$=6.895 GPa G_{13} = 6.205 GPa	G' = -3.3691 β 2+4.9975×103 β +0.873×106
h_i=1 mm (i=t, b)	$\upsilon_{12} = \upsilon_{13}$ = 0.22, υ_{23}=0.49	G''=-0.9 β 2+0.8124×103 β +0.1855×106

Table .4. The first natural frequency and the corresponding modal loss factor for the first few mode numbers for selected MR core layer thickness parameters (h_c / h_t = 1, 4,8), geometric aspect ratios (a/b = 1, 2, 4,8), and magnetic field strengths (β = 0, 100, 200, 300,400,450,500,600 Gauss).

[0/90/0/core/0/90/0]			β=0 Gauss		β=100 Gauss		β= 200Gauss		β= 300Gauss	
Mode	h_c / h_t	a/b	ω(Hz)	η_v	ω(Hz)	η_v	ω(Hz)	η_v	ω(Hz)	η_v
		۱	61.1592	0.1149	68.8699	0.1070	74.048	0.0985	77.6522	0.0904
	۱	۲	۱۰۲/۰۹۷	۰/۱۲۶۱	۱۱۶/۷۰۱	۰/۱۲۴۳	۱۲۷/۱۴	۰/۱۱۹۰	۱۳۴/۷۵۱	۰/۱۱۲۳
		۴	۲۳۹/۶۴۷	۰/۰۸۶۷	۲۶۴/۳۰۵	۰/۰۹۶۹	۲۸۳/۳۱۳	۰/۱۰۰۲	۲۹۷/۹۲۳	۰/۰۹۹۶
		۸	۷۵۲/۳۷۳	۰/۰۳۴۶	۷۸۴/۴۱۶	۰/۰۴۴۰	۸۱۰/۶۹	۰/۰۴۹۶	۸۳۱/۷۹۲	۰/۰۵۲۴
		۱	۴۰/۲۳۹۱	۰/۱۶۳۰	۴۷/۲۴۳۴	۰/۱۳۹۴	۵۱/۸۰۹۷	۰/۱۲۳۳	۵۴/۹۴	۰/۱۱۰۷
(1,1)	۴	۲	۶۶/۹۴۶۱	۰/۱۸۰۳	۸۰/۲۲۰۹	۰/۱۶۱۳	۸۹/۳۹۶۱	۰/۱۴۷۵	۹۵/۹۶۹۷	۰/۱۳۵۷
		۴	۱۳۴/۲۸۵	۰/۱۶۹۸	۱۶۰/۱۲۹	۰/۱۶۲۳	۱۷۸/۹۱۵	۰/۱۵۴۳	۱۹۲/۸۸۳	۰/۱۴۵۹
		۸	۳۲۱/۷۵۷	۰/۱۱۶۳	۳۶۵/۷۶۹	۰/۱۲۴۴	۳۹۹/۳۹۱	۰/۱۲۵۸	۴۲۵/۱۶۵	۰/۱۲۳۴
		۱	۳۵/۸۰۶۶	۰/۱۶۳۲	۴۱/۹۱۷	۰/۱۳۴۱	۴۵/۷۵۹۸	۰/۱۱۵۸	۴۸/۳۳۰۱	۰/۱۰۲۳
		۲	۶۰/۴۷۹۹	۰/۱۸۶۹	۷۲/۷۲۵۹	۰/۱۶۱۸	۸۰/۹۸۶	۰/۱۴۵۱	۸۶/۸۰۳۱	۰/۱۳۱۸
	۸	۴	۱۱۷/۳۳۵	۰/۱۹۶۳	۱۴۲/۹۵۸	۰/۱۷۸۰	۱۶۱/۱۸	۰/۱۶۵۱	۱۷۴/۵۵۷	۰/۱۵۳۸
		۸	۲۴۵/۷۸۲	۰/۱۷۸۴	۲۹۵/۵۴۶	۰/۱۷۰۰	۳۳۱/۹۶۱	۰/۱۶۲۰	۳۵۹/۲۱۸	۰/۱۵۳۵
		۱	102.097	0.1261	116.701	0.1243	127.14	0.1190	134.751	0.1123
		۲	۱۷۸/۶۶۶	۰/۰۶۹۵	۱۹۳/۳۸	۰/۰۷۸۵	۲۰۴/۶۲۴	۰/۰۸۱۵	۲۱۳/۱۸۸	۰/۰۸۱۱
	۱	۴	۲۹۵/۹۱	۰/۰۶۷۰	۳۱۹/۷۲۴	۰/۰۷۸۱	۳۳۸/۴۱۱	۰/۰۸۳۰	۳۵۲/۹۴۲	۰/۰۸۳۹
		۸	۷۹۴/۲۴۱	۰/۰۳۲۴	۸۲۶/۰۱	۰/۰۴۱۴	۸۵۲/۱۱	۰/۰۴۶۹	۸۷۳/۱۰۲	۰/۰۴۹۷
		۱	۶۶/۹۴۶۱	۰/۱۸۰۳	۸۰/۲۲۰۹	۰/۱۶۱۳	۸۹/۳۹۶۱	۰/۱۴۷۵	۹۵/۹۶۹۷	۰/۱۳۵۷
(1,2)	۴	۲	۹۳/۸۷۶۳	۰/۱۵۴۹	۱۱۰/۲۹۷	۰/۱۴۸۴	۱۲۲/۰۸۲	۰/۱۴۰۷	۱۳۰/۷۳۷	۰/۱۳۲۴
		۴	۱۵۲/۲۷	۰/۱۵۵۷	۱۷۹/۳۶۳	۰/۱۵۲۷	۱۹۹/۲۵۲	۰/۱۴۷۱	۲۱۴/۱۲	۰/۱۴۰۱
		۸	۳۳۴/۷۷۶	۰/۱۱۲۳	۳۷۹/۰۹۲	۰/۱۲۱۱	۴۱۳/۰۴	۰/۱۲۲۹	۴۳۹/۱۰۵	۰/۱۲۰۸
		۱	۶۰/۴۷۹۹	۰/۱۸۶۹	۷۲/۷۲۵۹	۰/۱۶۱۸	۸۰/۹۸۶	۰/۱۴۵۱	۸۶/۸۰۳۱	۰/۱۳۱۸
	۸	۲	۷۹/۷۶۳۲	۰/۱۸۵۶	۹۶/۰۷۶۸	۰/۱۶۶۱	۱۰۷/۴۱۳	۰/۱۵۲۲	۱۱۵/۵۷۶	۰/۱۴۰۳
		۴	۱۲۸/۸۹۶	۰/۱۹۲۰	۱۵۶/۵۲۲	۰/۱۷۵۶	۱۷۶/۲۴	۰/۱۶۳۶	۱۹۰/۷۴۶	۰/۱۵۲۷
		۸	۲۵۲/۸۴۱	۰/۱۷۶۲	۳۰۳/۴۶۱	۰/۱۶۸۶	۳۴۰/۵۴	۰/۱۶۰۸	۳۶۸/۳۰۷	۰/۱۵۲۵
(2,1)	۱	۱	152.042	۰/۰۵۸۳	۱۶۲/۵۶۲	۰/۰۶۶۹	۱۷۰/۶۲۵	۰/۰۷۰۱	۱۷۶/۷۷۶	۰/۰۷۰۳۳

		۲	۲۳۹/۶۴۷	۰/۰۸۶۷	۲۶۴/۳۰۵	۰/۰۹۶۹	۲۸۳/۳۱۳	۰/۱۰۰۲	۲۹۷/۹۲۳	۰/۰۹۹۶
		۴	۷۵۲/۳۷۳	۰/۰۳۴۶	۷۸۴/۴۱۶	۰/۰۴۴۰	۸۱۰/۶۹	۰/۰۴۹۶	۸۳۱/۷۹۲	۰/۰۵۲۴
		۸	۲۷۷۳/۹	۰/۰۱۰۰	۲۸۰۸/۸۵	۰/۰۱۳۶	۲۸۳۸/۳۷	۰/۰۱۶۱	۲۸۶۲/۶۴	۰/۰۱۷۷
		۱	۷۵/۹۲۲۲	۰/۱۴۳۸	۸۸/۲۷۴۸	۰/۱۳۹۴	۹۷/۱۴۱۱	۰/۱۳۲۹	۱۰۳/۶۵	۰/۱۲۵۵
	۴	۲	۱۳۴/۲۸۵	۰/۱۶۹۸	۱۶۰/۱۲۹	۰/۱۶۲۳	۱۷۸/۹۱۵	۰/۱۵۴۳	۱۹۲/۸۸۳	۰/۱۴۵۹
		۴	۳۲۱/۷۵۷	۰/۱۱۶۳	۳۶۵/۷۶۹	۰/۱۲۴۴	۳۹۹/۳۹۱	۰/۱۲۵۸	۴۲۵/۱۶۵	۰/۱۲۳۴
		۸	۹۷۳/۲۸۱	۰/۰۵۰۴	۱۰۳۳/۳۱	۰/۰۶۲۱	۱۰۸۱/۹۵	۰/۰۶۸۵	۱۱۲۰/۶۹	۰/۰۷۱۲
		۱	۶۲/۹۹۶۹	۰/۱۷۹۵	۷۵/۴۳۷۷	۰/۱۶۱۰	۸۴/۰۵۳۵	۰/۱۴۷۶	۹۰/۲۴۵	۰/۱۳۶۲
	۸	۲	۱۱۷/۳۳۵	۰/۱۹۶۳	۱۴۲/۹۵۸	۰/۱۷۸۰	۱۶۱/۱۸	۰/۱۶۵۱	۱۷۴/۵۵۷	۰/۱۵۳۸
		۴	۲۴۵/۷۸۲	۰/۱۷۸۴	۲۹۵/۵۴۶	۰/۱۷۰۰	۳۳۱/۹۶۱	۰/۱۶۲۰	۳۵۹/۲۱۸	۰/۱۵۳۵
		۸	۵۸۸/۵۳۸	۰/۱۲۳۸	۶۷۴/۰۰۹	۰/۱۳۱۰	۷۳۹/۱۴۲	۰/۱۳۱۶	۷۸۹/۰۳۵	۰/۱۲۸۷
		۱	۱۷۸/۶۶۶	۰/۰۶۹۵	۱۹۳/۳۸	۰/۰۷۸۵	۲۰۴/۶۲۴	۰/۰۸۱۵	۲۱۳/۱۸۸	۰/۰۸۱۱
	۱	۲	۲۹۵/۹۱	۰/۰۶۷۰	۳۱۹/۷۲۴	۰/۰۷۸۱	۳۳۸/۴۱۱	۰/۰۸۳۰	۳۵۲/۹۴۲	۰/۰۸۳۹
		۴	۷۹۴/۲۴۱	۰/۰۳۲۴	۸۲۶/۰۱	۰/۰۴۱۴	۸۵۲/۱۱	۰/۰۴۶۹	۸۷۳/۱۰۲	۰/۰۴۹۷
		۸	۲۸۱۰/۰۳	۰/۰۰۹۹	۲۸۴۴/۹۳	۰/۰۱۳۴	۲۸۷۴/۴۱	۰/۰۱۵۹	۲۸۹۸/۶۵	۰/۰۱۷۴
		۱	۹۳/۸۷۶۳	۰/۱۵۴۹	۱۱۰/۲۹۷	۰/۱۴۸۴	۱۲۲/۰۸۲	۰/۱۴۰۷	۱۳۰/۷۳۷	۰/۱۳۲۴
	۴	۲	۱۵۲/۲۷	۰/۱۵۵۷	۱۷۹/۳۶۳	۰/۱۵۲۷	۱۹۹/۲۵۲	۰/۱۴۷۱	۲۱۴/۱۲	۰/۱۴۰۱
(2,2)		۴	۳۳۴/۷۷۶	۰/۱۱۲۳	۳۷۹/۰۹۲	۰/۱۲۱۱	۴۱۳/۰۴	۰/۱۲۲۹	۴۳۹/۱۰۵	۰/۱۲۰۸
		۸	۹۸۴/۵۸	۰/۰۴۹۹	۱۰۴۴/۶۲	۰/۰۶۱۵	۱۰۹۳/۳	۰/۰۶۷۹	۱۱۳۲/۰۹	۰/۰۷۰۶
		۱	۷۹/۷۶۳۲	۰/۱۸۵۶	۹۶/۰۷۶۸	۰/۱۶۶۱	۱۰۷/۴۱۳	۰/۱۵۲۲	۱۱۵/۵۷۶	۰/۱۴۰۳
	۸	۲	۱۲۸/۸۹۶	۰/۱۹۲۰	۱۵۶/۵۲۲	۰/۱۷۵۶	۱۷۶/۲۴	۰/۱۶۳۶	۱۹۰/۷۴۶	۰/۱۵۲۷
		۴	۲۵۲/۸۴۱	۰/۱۷۶۲	۳۰۳/۴۶۱	۰/۱۶۸۶	۳۴۰/۵۴	۰/۱۶۰۸	۳۶۸/۳۰۷	۰/۱۵۲۵
		۸	۵۹۳/۸۰۸	۰/۱۲۳۰	۶۷۹/۵۳۲	۰/۱۳۰۳	۷۴۴/۸۹۲	۰/۱۳۱۱	۷۹۴/۹۷۲	۰/۱۲۸۳

Table 5. Displays the computed first natural frequency and the corresponding modal loss factor for the first few mode numbers (m ,n =1,2), for selected MR core layer thickness parameters(h_c / h_t = 1,4,8), geometric aspect ratios (a/b = 1, 2, 4,8), and magnetic field strengths (β = 0, 100, 200, 300,400,450,500,600 Gauss).

[0/90/0/core/0/90/0]			β=400 Gauss		β= 450Gauss		β=500 Gauss		β= 600Gauss	
Mode	h_c / h_t	a/b	ω(Hz)	η_v	ω(Hz)	η_v	ω(Hz)	η_v	ω(Hz)	η_v
		۱	80.1662	0.0828	۸۱/۱۰۳۸	۰/۰۷۹۰	81.8597	0.0725	۸۲/۸۸۸۸	۰/۰۶۷۴
	۱	۲	۱۴۰/۲۴۸	۰/۱۰۴۹	۱۴۲/۳۴۲	۰/۱۰۰۸	۱۴۴/۰۵	۰/۰۹۶۶	۱۴۶/۴۰۷	۰/۰۸۷۳
		۴	۳۰۸/۸۹۲	۰/۰۹۶۴	۳۱۳/۱۶۹	۰/۰۹۳۹	۳۱۶/۷	۰/۰۹۰۹	۳۲۱/۶۵۳	۰/۰۸۳۳
		۸	۸۴۸/۱۵۱	۰/۰۵۲۹	۸۵۴/۶۵۲	۰/۰۵۲۴	۸۶۰/۰۷۵	۰/۰۵۱۳	۸۶۷/۷۷۶	۰/۰۴۷۹
		۱	۵۷/۱۰۳۹	۰/۰۹۹۹	۵۷/۹۰۷۲	۰/۰۹۴۹	۵۸/۵۵۳۳	۰/۰۹۰۰	۵۹/۴۳۰۳	۰/۰۸۰۳
(1,1)		۲	۱۰۰/۶۶۸	۰/۱۲۴۷	۱۰۲/۴۴۸	۰/۱۱۹۲	۱۰۳/۸۹۶	۰/۱۱۳۷	۱۰۵/۸۸۹	۰/۱۰۲۲
	۴	۴	۲۰۳/۱۵۶	۰/۱۳۶۷	۲۰۷/۱۱۷	۰/۱۳۱۷	۲۱۰/۳۶۹	۰/۱۲۶۳	۲۱۴/۹	۰/۱۱۴۵
		۸	۴۴۴/۵۱۶	۰/۱۱۸۴	۴۵۲/۰۶۶	۰/۱۱۵۰	۴۵۸/۳۰۴	۰/۱۱۱۱	۴۶۷/۰۶۳	۰/۱۰۱۶
		۱	۵۰/۰۷۵۹	۰/۰۹۱۴	۵۰/۷۱۷۳	۰/۰۸۶۴	۵۱/۲۳۰۴	۰/۰۸۱۷	۵۱/۹۲۲۵	۰/۰۷۲۶
		۲	۹۰/۹۰۸۵	۰/۱۲۰۱	۹۲/۴۵۱۹	۰/۱۱۴۴	۹۳/۷۰۱۹	۰/۱۰۸۹	۹۵/۴۱۳۵	۰/۰۹۷۵
	۸	۴	۱۸۴/۳۱۲	۰/۱۴۲۷	۱۸۸/۰۵۵	۰/۱۳۷۰	۱۹۱/۱۲	۰/۱۳۱۱	۱۹۵/۳۷۸	۰/۱۱۸۴
		۸	۳۷۹/۳۸۱	۰/۱۴۴۱	۳۸۷/۱۸۶	۰/۱۳۹۰	۳۹۳/۶۰۹	۰/۱۳۳۵	۴۰۲/۵۸۴	۰/۱۲۱۱
		۱	140.248	0.1004	142.342	0.1001	144.05	0.0966	۱۴۶/۴۰۷	۰/۰۸۷۳
		۲	219.566	0.0784	222.038	0.0764	224.073	0.0739	226.915	۰/۰۶۷۷
	۱	۴	۳۶۳/۹۳۸	۰/۰۸۲۱	۳۶۸/۲۴۴	۰/۰۸۰۴	۳۷۱/۸۰۸	۰/۰۷۸۱	۳۷۶/۸۲	۰/۰۷۱۹
		۸	۸۸۹/۳۹۳	۰/۰۵۰۲	۸۹۵/۸۷۲	۰/۰۴۹۸	۹۰۱/۲۷۷	۰/۰۴۸۸	۹۰۸/۹۵۸	۰/۰۴۵۶
		۱	۱۰۰/۶۶۸	۰/۱۲۴۷	۱۰۲/۴۴۸	۰/۱۱۹۲	۱۰۳/۸۹۶	۰/۱۱۳۷	۱۰۵/۸۸۹	۰/۱۰۲۲
(1,2)	۴	۲	۱۳۷/۰۳۵	۰/۱۲۳۵	۱۳۹/۴۴۷	۰/۱۱۸۸	۱۴۱/۴۱۹	۰/۱۱۳۸	۱۴۴/۱۵۳	۰/۱۰۲۹
		۴	۲۲۵/۰۹۱	۰/۱۳۱۸	۲۲۹/۳۲۸	۰/۱۲۷۲	۲۳۲/۸۱۱	۰/۱۲۲۲	۲۳۷/۶۶۸	۰/۱۱۰۹
		۸	۴۵۸/۶۹۳	۰/۱۱۶۱	۴۶۶/۳۴	۰/۱۱۲۹	۴۷۲/۶۶	۰/۱۰۹۲	۴۸۱/۵۳۵	۰/۰۹۹۹
		۱	۹۰/۹۰۸۵	۰/۱۲۰۱	۹۲/۴۵۱۹	۰/۱۱۴۴	۹۳/۷۰۱۹	۰/۱۰۸۹	۹۵/۴۱۳۵	۰/۰۹۷۵
	۸	۲	۱۲۱/۴۳۶	۰/۱۲۹۲	۱۲۳/۶۶۲	۰/۱۲۳۶	۱۲۵/۴۷۵	۰/۱۱۸۰	۱۲۷/۹۷۵	۰/۱۰۶۱
		۴	۲۰۱/۳۳۸	۰/۱۴۱۹	۲۰۵/۴۰۶	۰/۱۳۶۳	۲۰۸/۷۳۸	۰/۱۳۰۵	۲۱۳/۳۶۹	۰/۱۱۷۹
		۸	۳۸۸/۸۵۲	۰/۱۴۳۳	۳۹۶/۸۰۶	۰/۱۳۸۲	۴۰۳/۳۵۲	۰/۱۳۲۷	۴۱۲/۴۹۸	۰/۱۲۰۴

	۱	۱	۱۸۱/۳۶۳	۰/۰۶۸۳	۱۸۳/۱۴۳	۰/۰۶۶۶	۱۸۴/۶۰۸	۰/۰۶۴۶	۱۸۶/۶۵۶	۰/۰۵۹۳
		۲	۳۰۸/۸۹۲	۰/۰۹۶۴	۳۱۳/۱۶۹	۰/۰۹۳۹	۳۱۶/۷	۰/۰۹۰۹	۳۲۱/۶۵۳	۰/۰۸۳۳
		۴	۸۴۸/۱۵۱	۰/۰۵۲۹	۸۵۴/۶۵۲	۰/۰۵۲۴	۸۶۰/۰۷۵	۰/۰۵۱۳	۸۶۷/۷۷۶	۰/۰۴۷۹
		۸	۲۸۸۱/۸۱	۰/۰۱۸۳	۲۸۸۹/۵۱	۰/۰۱۸۴	۲۸۹۵/۹۸	۰/۰۱۸۲	۲۹۰۵/۲۳	۰/۰۱۷۲
(2,1)	۴	۱	۱۰۸/۳۸۵	۰/۱۱۷۴	۱۱۰/۱۹۷	۰/۱۱۳	۱۱۱/۶۷۹	۰/۱۰۸۳	۱۱۳/۷۳۴	۰/۰۹۸۰
		۲	۲۰۳/۱۵۶	۰/۱۳۶۷	۲۰۷/۱۱۷	۰/۱۳۱۷	۲۱۰/۳۶۹	۰/۱۲۶۳	۲۱۴/۹	۰/۱۱۴۵
		۴	۴۴۴/۵۱۶	۰/۱۱۸۴	۴۵۲/۰۶۶	۰/۱۱۵۰	۴۵۸/۳۰۴	۰/۱۱۱۱	۴۶۷/۰۶۳	۰/۱۰۱۶
		۸	۱۱۵۰/۵۵	۰/۰۷۱۱	۱۱۶۲/۳۸	۰/۰۷۰۱	۱۱۷۲/۲۳	۰/۰۶۸۵	۱۱۸۶/۱۹	۰/۰۶۳۶
	۸	۱	۹۴/۶۸۴۳	۰/۱۲۵۴	۹۶/۳۶۹۸	۰/۱۲۰۱	۹۷/۷۴۲۴	۰/۱۱۴۷	۹۹/۶۳۴۹	۰/۱۰۳۲
		۲	۱۸۴/۳۱۲	۰/۱۴۲۷	۱۸۸/۰۵۵	۰/۱۳۷۰	۱۹۱/۱۲	۰/۱۳۱۱	۱۹۵/۳۷۸	۰/۱۱۸۴
		۴	۳۷۹/۳۸۱	۰/۱۴۴۱	۳۸۷/۱۸۶	۰/۱۳۹۰	۳۹۳/۶۰۹	۰/۱۳۳۵	۴۰۲/۵۸۴	۰/۱۲۱۱
		۸	۸۲۶/۴۹۲	۰/۱۲۳۳	۸۴۱/۱۱	۰/۱۱۹۸	۸۵۳/۱۹	۰/۱۱۵۶	۸۷۰/۱۵۳	۰/۱۰۵۷
	۱	۱	۲۱۹/۵۶۶	۰/۰۷۸۴	۲۲۲/۰۳۸	۰/۰۷۶۴	۲۲۴/۰۷۳	۰/۰۷۳۹	۲۲۶/۹۱۵	۰/۰۶۷۷
		۲	۳۶۳/۹۳۸	۰/۰۸۲۱	۳۶۸/۲۴۴	۰/۰۸۰۴	۳۷۱/۸۰۸	۰/۰۷۸۱	۳۷۶/۸۲	۰/۰۷۱۹
		۴	۸۸۹/۳۹۳	۰/۰۵۰۲	۸۹۵/۸۷۲	۰/۰۴۹۸	۹۰۱/۲۷۷	۰/۰۴۸۸	۹۰۸/۹۵۸	۰/۰۴۵۶
		۸	۲۹۱۷/۷۹	۰/۰۱۸۱	۲۹۲۵/۸۴	۰/۰۱۸۱	۲۹۳۱/۹۴	۰/۰۱۷۹	۲۹۴۱/۱۹	۰/۰۱۶۹
(2,2)	۴	۱	۱۳۷/۰۳۵	۰/۱۲۳۵	۱۳۹/۴۴۷	۰/۱۱۸۸	۱۴۱/۴۱۹	۰/۱۱۳۸	۱۴۴/۱۵۳	۰/۱۰۲۹
		۲	۲۲۵/۰۹۱	۰/۱۳۱۸	۲۲۹/۳۲۸	۰/۱۲۷۲	۲۳۲/۸۱۱	۰/۱۲۲۲	۲۳۷/۶۶۸	۰/۱۱۰۹
		۴	۴۵۸/۶۹۳	۰/۱۱۶۱	۴۶۶/۳۴	۰/۱۱۲۹	۴۷۲/۶۶	۰/۱۰۹۲	۴۸۱/۵۳۵	۰/۰۹۹۹
		۸	۱۱۶۱/۹۹	۰/۰۷۰۵	۱۱۷۳/۸۴	۰/۰۶۹۵	۱۱۸۳/۷	۰/۰۶۷۹	۱۱۹۷/۶۹	۰/۰۶۳۱
	۸	۱	۱۲۱/۴۳۶	۰/۱۲۹۲	۱۲۳/۶۶۲	۰/۱۲۳۶	۱۲۵/۴۷۵	۰/۱۱۸۰	۱۲۵/۹۷۵	۰/۱۰۶۱
		۲	۲۰۱/۳۳۸	۰/۱۴۱۹	۲۰۵/۴۰۶	۰/۱۳۶۳	۲۰۸/۷۳۸	۰/۱۳۰۵	۲۱۳/۳۶۹	۰/۱۱۷۹
		۴	۳۸۸/۸۵۲	۰/۱۴۳۳	۳۹۶/۸۰۶	۰/۱۳۸۲	۴۰۳/۳۵۲	۰/۱۳۲۷	۴۱۲/۴۹۸	۰/۱۲۰۴
		۸	۸۳۲/۵۷۷	۰/۱۲۲۹	۸۴۷/۲۵۴	۰/۱۱۹۴	۸۵۹/۳۸۳	۰/۱۱۵۳	۸۷۶/۴۱۷	۰/۱۰۵۴

The variation of the modal loss factor η_v can be understood within the framework of the Modal Strain Energy (MSE) method. The modal loss factor for the n-th mode is expressed as: $\eta_v = \frac{W_n^{\text{core}}}{W_n^{\text{total}}} \cdot \eta_{\text{core}}$.

where $W_n^{\text{core}}$is the modal strain energy stored in the MR core, $W_n^{\text{total}}$is the total modal strain energy of the sandwich panel, and $\eta_{\text{core}}$is the material loss factor of the MR core.

The MR fluid core is characterized by a complex shear modulus of the form: $G = G' + iG''$.

where $G'$is the storage modulus (representing the elastic stiffness component) and $G'' = \eta_{\text{core}} \cdot$

$G'$is the loss modulus (representing the viscous dissipation capacity). Both $G'$and $G''$are strongly dependent on the applied magnetic field intensity β, and this field-dependence is the primary mechanism through which the modal loss factor of the sandwich panel is tunable.

Under increasing magnetic field, G'increases significantly, stiffening the MR core and thereby increasing the shear strain energy concentrated within it. However, the ratio G''/G' does not increase monotonically and may plateau or decrease at higher field intensities depending on the MR fluid composition. Consequently, the modal loss factor η_v reflects a competition between two effects:

1. Increased strain energy fraction in the core — as the core stiffens, a larger proportion of the total modal strain energy is stored in the MR layer, which tends to increase η_v.

2. Reduction in the intrinsic loss factor η_{core} at high field intensities, the dissipation efficiency of the MR fluid may decrease, which tends to decrease η_v.

The non-monotonic or mode-dependent variation of η_v observed in the results is therefore a direct consequence of this interplay. Higher-order modes, which exhibit greater shear deformation in the core relative to bending of the face sheets, generally yield a higher $W_n^{\text{core}}/W_n^{\text{total}}$ratio, and are thus more sensitive to changes in the complex shear modulus of the MR core.

The modal loss factor of the sandwich panel is governed not by the magnetic field intensity directly, but by the relative rate of change of the storage modulus G' and the loss modulus G'' of the MR core. These two quantities respond differently to an applied magnetic field, and it is their ratio that ultimately determines the dissipative behaviour of the system.

The material loss factor of the MR core is defined as: $\eta_{\text{core}} = \frac{G''}{G'} = \tan\ \delta$
As the magnetic field intensity H increases, both G' and G'' increase; however, they do not increase at the same rate. Three distinct regimes can be identified:

Regime 1 — Low field intensity: At low field levels, G'' increases at a proportionally higher rate than G', increasing in $\tan\delta$ and consequently an increase in η_{core}. In this regime, the modal loss factor η_v of the panel tends to increase with the applied field.

Regime 2 — Intermediate field intensity: As the field increases further, the rates of increase of G' and G'' become comparable. The storage modulus begins to dominate, as the magnetorheological effect progressively stiffens the core. The ratio G''/G' approaches a plateau, and the modal loss factor stabilises or exhibits only marginal variation.

Regime 3 — High field intensity (saturation): Near magnetic saturation, G' continues to increase or saturates, while G'' may plateau or even decrease. This causes $\tan\delta$ to decline, reducing η_{core} and therefore the panel-level modal loss factor η_v.

This behavior is further modulated by the modal strain energy distribution. Even if η_{core} decreases at high field intensities, the simultaneous stiffening of the core increases the proportion of strain energy stored within it, $W_n^{\text{core}}/W_n^{\text{total}}$ increases. The net effect on η_n is therefore determined by the competition between the decrease in η_{core} and the increase in the core strain energy fraction. Depending on which effect dominates, η_n may increase, decrease, or exhibit a non-monotonic trend with respect to the applied magnetic field — consistent with the results reported in the present study.

This clarification has been incorporated into the revised manuscript to ensure a more physically complete and accurate interpretation of the observed loss factor behavior.

The increased sensitivity of higher vibration modes to the applied magnetic field intensity can be physically attributed to the mode-dependent distribution of shear deformation within the MR core and the corresponding variation in the modal strain energy (MSE) fraction concentrated in the core layer.

The physical reasoning proceeds as follows:

Shear deformation and mode shape curvature: Higher vibration modes are characterized by shorter half-wavelengths and greater spatial curvature in their mode shapes. For a sandwich panel with soft-core construction, the transverse shear deformation is predominantly accommodated by the compliant MR core rather than the stiff composite face sheets. As the mode number increases, the number of inflection points in the mode shape increases, and the magnitude of the transverse shear strain within the core grows correspondingly. This results in a disproportionately larger fraction of the total strain energy being stored in the MR core for higher modes.

Modal strain energy participation: As observed from the present results across the field levels B= 400, 450, 500, and 600 Gauss, the shift in natural frequency and the variation in modal loss factor η_v become more pronounced with increasing mode number. This is consistent with the fact that, for higher modes, a greater proportion of W_n^{total} resides in the MR core — the very layer whose mechanical properties (G' and G'') are being actively altered by the magnetic field. Consequently, any field-induced change in the complex shear modulus $G = G' + iG''$ has a more significant impact on the overall dynamic response for higher modes than for lower ones.

Lower modes: For the fundamental and lower modes, the panel deformation is dominated by global bending, with relatively smooth mode shapes and lower shear strain gradients in the core. The face sheets — which are magnetically insensitive — carry a larger share of the strain energy. As a result, changes in the MR core properties produce only a modest effect on the natural frequency and loss factor of these modes.

Higher modes: In contrast, for higher-order modes — as clearly evidenced by the tabulated results across the (1,1), (1,2), (2,1), and (2,2) mode families — the core strain energy fraction $W_n^{\text{core}}/W_n^{\text{total}}$ is substantially larger. The stiffening of the MR core with increasing field intensity therefore produces a more pronounced upward shift in natural frequency and a more significant variation in modal loss factor. This enhanced tunability of higher modes is a desirable property for semi-active vibration control applications, where selective modal targeting is often required.

This mode-dependent behavior is fully consistent with classical sandwich beam and plate theory, wherein the contribution of core shear flexibility to the overall dynamic response increases with mode number, and confirms that the MR core is most effective as a controllable damping element for higher vibration modes.

The observed enhancement in the natural frequencies with the increase of magnetic field intensity is physically attributed to the stiffening

This increase is quite noticeable to the 400 Gauss value. On the other hand, increasing the magnetic field strength appears to have different effects on the modal loss factors, depending on the mode number. For the lower modes considered (m,n =1,2), the loss factor seems to decrease, and for the higher mode numbers, the loss factor seems to initially increase at low magnetic field strength, reach a peak at intermediate magnetic field magnitude, and subsequently decrease as the magnetic field strength is further enhanced. The generality of the problem showed an increase in the natural frequencies of the sandwich panel with the MR core with an increase in the intensity of the magnetic field. Of course, this increase in frequency only continues up to a certain level of magnetic field intensity and does not increase indefinitely. This limiting value is referred to as the saturation magnetic field intensity (β s), which in this research is approximately equal to 400 Gauss. Therefore, by creating a magnetic field whose intensity can be controlled, the natural frequencies and thus the vibrations of the structure can be controlled. The effect of changes in the magnetic field intensity, under simply supported (SS) boundary conditions, on the natural frequencies of an MR fluid sandwich panel is summarized in Figure 2. Results for the first four modes are shown for the following field intensities: 0, ...,600 Gauss. The findings consistently demonstrate that as the magnetic field increases, so do the natural frequencies corresponding to each mode.

effect of the Magnetorheological (MR) core. When an external magnetic field is applied, the MR particles within the core form chain-like structures along the field lines, which significantly increases the storage shear modulus of the material. Consequently, the transverse shear stiffness of the entire sandwich panel is enhanced, leading to a higher restoration force during vibration and, therefore, an upward shift in the natural frequencies.

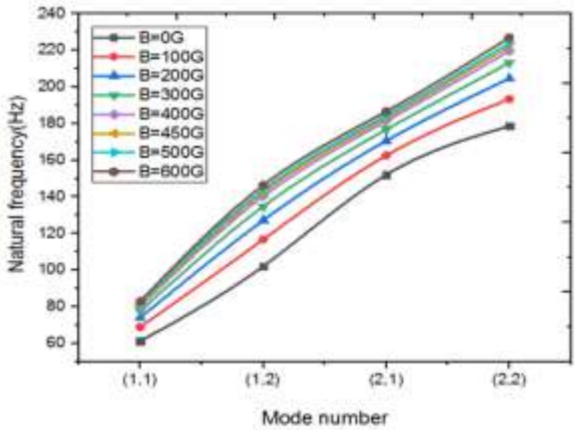

Figure 2. Effect of magnetic field intensity ($\boldsymbol{B}$) on the first four natural frequencies $\boldsymbol{\omega_n}$ of the MR-cored sandwich plate for $\boldsymbol{h_c/h_t = 1}$ and a square plate aspect ratio of $\boldsymbol{a/b = 1}$.

Results are presented for mode numbers. (m,n)= (1,1), (1,2), (2,1), and (2,2), illustrating the progressive upward shift in natural frequency with increasing applied field, attributable to the field-induced stiffening of the complex shear modulus Gof the MR core.

As observed in Fig. 2, the natural frequencies increase with the magnetic field intensity. This is physically attributed to the stiffening effect of the MR fluid core. Under an external magnetic field, the iron particles within the MR layer align into chain-like structures, which significantly enhances the complex shear modulus of the core. Consequently, the overall structural stiffness of the sandwich plate increases, leading to higher natural frequencies for all vibration modes.

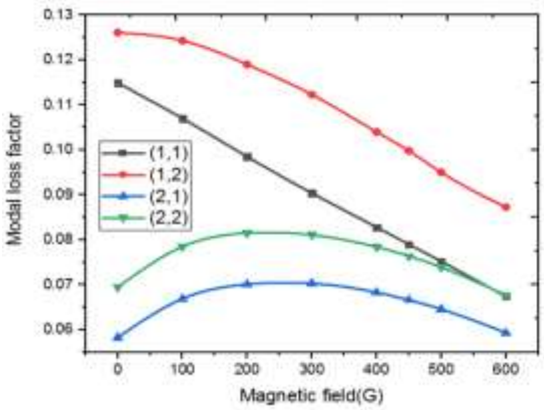

Figure 3. Influence of magnetic field on the modal loss factor η_v. for the first four vibration modes $(m، n)$= (1، 1), (1، 2), (2، 1), and (2، 2)of the MR-cored sandwich plate ($h_c/h_t = 1$, $a/b = 1$).

The modal loss factor in Fig. 3 exhibits a non-monotonic behavior for higher modes. This phenomenon can be interpreted through the competition between two mechanisms: the increase in the core's storage modulus and the variation in the modal strain energy (MSE) distribution. While a stronger magnetic field enhances the material's intrinsic damping capacity to a certain point, the resulting increase in stiffness may shift the strain energy away from the MR core towards the elastic face sheets. When the reduction in the energy fraction stored in the MR layer outweighs the increase in its loss modulus, a decline in the overall modal loss factor is observed.

٤.3. *Influences of the MR layer thickness*

A comparison of the natural frequencies of the sandwich panel with different thicknesses of the MR layer at different magnetic fields for the simply supported end conditions for the first mode has been performed, and the results are shown in table5.

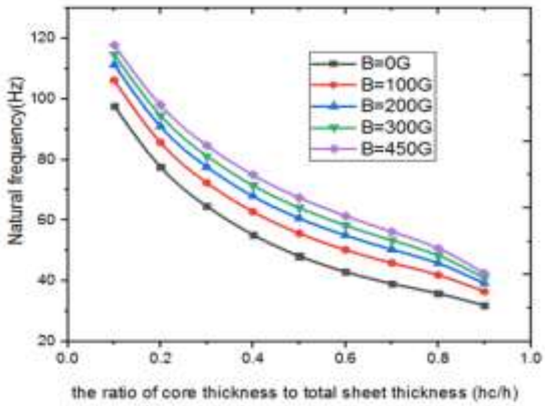

Figure 4. Influence of the MR core-to-total thickness ratio h_c/h on the natural frequencies $\boldsymbol{\omega_n}$of the MR-cored sandwich plate under simply supported boundary conditions, evaluated across magnetic field intensities, for a square plate geometry ($a/b = 1$).

The results generally show a decrease in the natural frequencies with an increase in the thickness of the MR layer. A significant variation can be observed in higher modes compared to that of lower modes. This can be attributed to the fact that the relative variation in the mass of the structure is higher than that of the stiffness when the thickness of the MR fluid layer increases.

The observed decrease in natural frequencies with an increase in the MR-core thickness can be physically attributed to the trade-off between the structural stiffness and the total mass of the sandwich panel. Although increasing the core thickness typically increases the moment of inertia, the MR core is significantly more compliant (softer) than the high-stiffness composite face sheets. Consequently, the increment in the overall stiffness is marginal compared to the linear increase in the total mass of the panel. This leads to a reduction in the overall stiffness-to-mass ratio, which results in a downward shift of the natural frequencies, as governed by the fundamental relationship $\boldsymbol{f_n \propto \sqrt{k/m}}$.

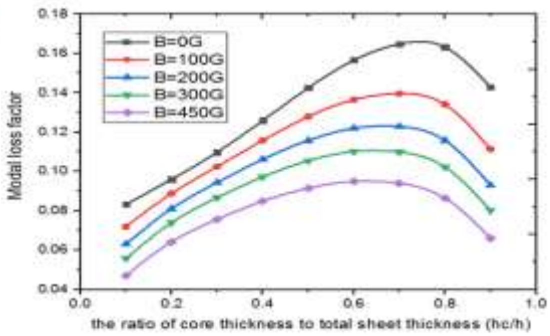

Figure 5. Influence of the MR core-to-total thickness ratio h_c/hon the modal loss factor η_v of the MR-cored sandwich plate under simply supported boundary conditions, evaluated across magnetic field intensities of B= 0, 100, 200, 300, and 450 Gauss, for a square plate geometry ($a/b = 1$).

Figure 5 illustrates the influence of the core-to-total thickness ratio h_c/h on the modal loss factor. It is observed that the loss factor initially increases with h_c/h , reaches a peak at approximately h_c/h ≈0.7 and then begins to decline. The physical interpretation of this trend lies in the trade-off between the volume of the dissipative MR material and the structural stiffness. Initially, increasing the core thickness provides more MR material to dissipate energy. However, beyond a certain ratio, the reduction in the facesheets' thickness (which provides the necessary constraint for shear deformation in the core) leads to a decrease in the shear strain levels within the MR layer. Since the damping in sandwich structures primarily depends on the interfacial shear strain, an excessively thick core with very thin face sheets fails to undergo significant shearing, thereby reducing the overall modal loss factor.

Table 5. The first natural frequency and the corresponding modal loss factor for the first mode numbers for selected MR core layer thickness parameters (h_c / h = 0.1,...,0.9), geometric aspect ratios (a/b = 1,2,4,8), and magnetic field strengths (G = 0, 100,200,300, 450 Gauss).

[0/90/0/core/0/90/0]			β=0 Gauss		β=100 Gauss		β= 200Gauss		β= 300Gauss		β= 450Gauss	
Mode	h_c / h	a/b	$\omega(Hz)$	η_v	$\omega(Hz)$	η_v	$\omega(Hz)$	η_v	$\omega(Hz)$	η_v	$\omega(Hz)$	η_v
(1,1)	۰/۱	۱	97.7257	0.0833	106.208	0.0720	111.393	0.0631	114.773	0.0559	117.838	0.0472
		۲	۱۶۸/۵۷۴	۰/۱۰۶۱	۱۸۸/۲۶۷	۰/۱۰۰۱	۲۰۱/۵۳۱	۰/۰۹۲۷	۲۱۰/۷۶۹	۰/۰۸۵۴	۲۱۹/۶۱۱	۰/۰۷۴۷
		۴	۴۰۹/۳۳۵	۰/۰۷۸۷	۴۴۷/۲۴۱	۰/۰۸۷۰	۴۷۵/۹۱۹	۰/۰۸۹۱	۴۹۷/۶۲	۰/۰۸۷۹	۵۱۹/۹۲۷	۰/۰۸۲۱
		۸	۱۳۰۴/۱۵	۰/۰۳۱۸	۱۳۵۵/۱۴	۰/۰۴۰۴	۱۳۹۶/۷۶	۰/۰۴۵۵	۱۴۳۰/۰۶	۰/۰۴۸۰	۱۴۶۶	۰/۰۴۷۹
	۰/۲	۱	۷۷/۵۸۴۶	۰/۰۹۶۰	۸۵/۶۶۹۷	۰/۰۸۸۸	۹۰/۹۷	۰/۰۸۱۱	۹۴/۵۹۱۵	۰/۰۷۴۰	۹۸/۰۰۳۴	۰/۰۶۴۲
		۲	۱۳۰/۸۴۶	۰/۱۱۰۱	۱۴۷/۱۴۳	۰/۱۰۹۲	۱۵۸/۶۷۴	۰/۱۰۴۶	۱۶۶/۹۹۹	۰/۰۹۸۶	۱۷۵/۲۲	۰/۰۸۸۲
		۴	۳۱۷/۹۱۵	۰/۰۷۳۵	۳۴۵/۷۶۵	۰/۰۸۳۸	۳۶۷/۳۲۱	۰/۰۸۷۷	۳۸۳/۹۱۳	۰/۰۸۷۷	۴۰۱/۲۳۲	۰/۰۸۳۲
		۸	۱۰۲۹/۲۳	۰/۰۲۷۹	۱۰۶۴/۷	۰/۰۳۶۰	۱۰۹۳/۹۲	۰/۰۴۱۰	۱۱۱۷/۴۷	۰/۰۴۳۶	۱۱۴۳/۰۶	۰/۰۴۳۹
	۰/۳	۱	۶۴/۶۱۵۹	۰/۱۰۹۸	۷۲/۳۹۲۴	۰/۱۰۲۵	۷۷/۶۰۲	۰/۰۹۴۴	۸۱/۲۱۹۹	۰/۰۸۶۷	۸۴/۶۷۷۲	۰/۰۷۵۷
		۲	۱۰۸/۰۶۸	۰/۱۲۱۲	۱۲۲/۹۳۹	۰/۱۲۰۱	۱۳۳/۵۷	۰/۱۱۵۲	۱۴۱/۳۱۶	۰/۱۰۸۹	۱۴۹/۰۳۵	۰/۰۹۷۹
		۴	۲۵۶/۵۸	۰/۰۸۱۹	۲۸۱/۵۸۵	۰/۰۹۲۴	۳۰۰/۹۱۵	۰/۰۹۶۰	۳۱۵/۷۹۷	۰/۰۹۵۸	۳۳۱/۳۴۵	۰/۰۹۰۵
		۸	۸۱۴/۹۲۵	۰/۰۳۲۰	۸۴۷/۰۷۳	۰/۰۴۰۹	۸۷۳/۴۹۵	۰/۰۴۶۴	۸۹۴/۷۵۳	۰/۰۴۹۱	۹۱۷/۸۱۶	۰/۰۴۹۲
	۰/۴	۱	۵۵/۱۹۹۵	۰/۱۲۵۹	۶۲/۸۰۸۶	۰/۱۱۵۸	۶۷/۹۲۱	۰/۱۰۶۲	۷۱/۴۸۵	۰/۰۹۷۳	۷۴/۹۰۴۷	۰/۰۸۴۹
		۲	۹۱/۸۷۷۱	۰/۱۳۷۲	۱۰۶/۱۱۴	۰/۱۳۳۰	۱۱۶/۲۵۸	۰/۱۲۶۴	۱۲۳/۶۴۹	۰/۱۱۸۹	۱۳۱/۰۲	۰/۱۰۶۵
		۴	۲۰۹/۸۴۵	۰/۰۹۸۸	۲۳۴/۳۰۳	۰/۱۰۷۹	۲۵۳	۰/۱۱۰۱	۲۶۷/۳	۰/۱۰۸۶	۲۸۲/۱۷۲	۰/۱۰۱۵
		۸	۶۳۸/۶۷۶	۰/۰۴۱۸	۶۷۱/۴۵۶	۰/۰۵۲۴	۶۹۸/۱۵۲	۰/۰۵۸۴	۷۱۹/۴۸۵	۰/۰۶۱۱	۷۴۲/۴۹۷	۰/۰۶۰۶
	۰/۵	۱	۴۸/۱۸۳۹	۰/۱۴۲۵	۵۵/۶۵۰۹	۰/۱۲۷۹	۶۰/۶۳۵	۰/۱۱۵۸	۶۴/۱۰۰۲	۰/۱۰۵۵	۶۷/۴۲۰۵	۰/۰۹۱۵
		۲	۷۹/۹۸۴	۰/۱۵۵۲	۹۳/۸۷۶۸	۰/۱۴۶۰	۱۰۳/۶۸۵	۰/۱۳۶۸	۱۱۰/۷۹۸	۰/۱۲۷۷	۱۱۷/۸۷۴	۰/۱۱۳۵
		۴	۱۷۳/۹۵۲	۰/۱۲۲۷	۱۹۸/۸۱۹	۰/۱۲۸۱	۲۱۷/۵۰۲	۰/۱۲۷۴	۲۳۱/۶۵۱	۰/۱۲۳۶	۲۶۴/۲۵۸	۰/۱۱۴۱
		۸	۴۹۴/۴۷۳	۰/۰۵۹۵	۵۳۰/۲۲۲	۰/۰۷۱۶	۵۵۸/۸۵۶	۰/۰۷۷۷	۵۸۱/۴۷۳	۰/۰۷۹۹	۶۰۵/۶۳۳	۰/۰۷۷۷
	۰/۶	۱	۴۲/۹۶۴۲	۰/۱۵۶۶	۵۰/۲۰۹۴	۰/۱۳۶۵	۵۴/۹۸۶	۰/۱۲۲۰	۵۸/۲۸۳۷	۰/۱۱۰۲	۶۱/۴۲۷۲	۰/۰۹۵۰
		۲	۷۱/۳۱۷۸	۰/۱۷۱۷	۸۴/۸۸۷۴	۰/۱۵۶۷	۹۴/۳۵۱۶	۰/۱۴۴۶	۱۰۱/۱۷	۰/۱۳۳۸	۱۰۷/۹۲	۰/۱۱۸۱
		۴	۱۴۷/۳۷	۰/۱۵۱۲	۱۷۲/۹۰۱	۰/۱۴۹۵	۱۹۱/۷۰۲	۰/۱۴۴۷	۲۰۵/۷۸۱	۰/۱۳۸۱	۲۲۰/۲	۰/۱۲۵۷
		۸	۳۸۰/۶۰۶	۰/۰۸۸۹	۴۲۱/۰۲۲	۰/۱۰۰۵	۴۵۲/۵۷۵	۰/۱۰۴۸	۴۷۷/۰۸۳	۰/۱۰۴۹	۵۰۲/۹۱۷	۰/۰۹۹۶
	۰/۷	۱	۳۹/۰۴۴۳	۰/۱۶۴۸	۴۵/۸۸۷۴	۰/۱۳۹۶	۵۰/۳۱۸۵	۰/۱۲۲۹	۵۳/۳۴۲۴	۰/۱۰۹۹	۵۶/۱۹۸۳	۰/۰۹۴۰
		۲	۶۵/۰۹۶۷	۰/۱۸۳۴	۷۸/۱۸۲۳	۰/۱۶۲۷	۸۷/۱۸۱۹	۰/۱۴۸۱	۹۳/۶۰۸۷	۰/۱۳۵۸	۹۹/۹۲۵۵	۰/۱۱۹۱
		۴	۱۲۸/۹۹۳	۰/۱۷۸۲	۱۵۴/۹۰۶	۰/۱۶۷۶	۱۷۳/۶۲۹	۰/۱۵۸۳	۱۸۷/۵۰۵	۰/۱۴۹۰	۲۰۱/۶۰۹	۰/۱۳۳۹
		۸	۲۹۷/۵۷۵	۰/۱۳۱۹	۳۴۳/۳۴	۰/۱۳۷۰	۳۷۷/۹	۰/۱۳۶۲	۴۰۴/۲۱۷	۰/۱۳۲۳	۴۳۱/۵۵۳	۰/۱۲۲۳
	۰/۸	۱	۳۵/۸۰۶۶	۰/۱۶۳۲	۴۱/۹۱۷	۰/۱۳۴۱	۴۵/۷۵۹۸	۰/۱۱۵۸	۴۸/۳۳۰۱	۰/۱۰۲۳	۵۰/۷۱۷۳	۰/۰۸۶۴
		۲	۶۰/۴۷۹۹	۰/۱۸۶۹	۷۲/۷۲۵۹	۰/۱۶۱۸	۸۰/۹۸۶	۰/۱۴۵۱	۸۶/۸۰۳۱	۰/۱۳۱۸	۹۲/۴۵۱۹	۰/۱۱۴۴
		۴	۱۱۷/۳۳۵	۰/۱۹۶۳	۱۴۲/۹۵۸	۰/۱۷۸۰	۱۶۱/۱۸	۰/۱۶۵۱	۱۷۴/۵۵۷	۰/۱۵۳۸	۱۸۸/۰۵۵	۰/۱۳۷۰
		۸	۲۴۵/۷۸۲	۰/۱۷۸۴	۲۹۵/۵۴۶	۰/۱۷۰۰	۳۳۱/۹۶۱	۰/۱۶۲۰	۳۵۹/۲۱۸	۰/۱۵۳۵	۳۸۷/۱۸۶	۰/۱۳۹۰
	۰/۹	۱	۳۱/۸۵۶۴	۰/۱۴۲۹	۳۶/۴۴۸۴	۰/۱۱۱۴	۳۹/۱۵۵۷	۰/۰۹۳۰	۴۰/۸۸۸۴	۰/۰۸۰۲	۴۲/۴۴۰۸	۰/۰۶۶۲

		۲	۵۵/۸۹۵۸	۰/۱۷۶۳	۶۶/۳۲۹۱	۰/۱۴۷۰	۷۳/۰۶۱۸	۰/۱۲۸۵	۷۷/۶۴۹	۰/۱۱۴۵	۸۱/۹۷۶	۰/۰۹۷۶
		۴	۱۰۹/۹۰۲	۰/۲۰۰۲	۱۳۴/۱۰۵	۰/۱۷۷۱	۱۵۰/۹۸۸	۰/۱۶۱۹	۱۶۳/۲۰۸	۰/۱۴۹۳	۱۷۵/۳۸۱	۰/۱۳۱۷
		۸	۲۲۰/۷۵۷	۰/۲۰۴۹	۲۷۱/۲۱۷	۰/۱۸۵۸	۳۰۷/۴۲۱	۰/۱۷۲۹	۳۳۴/۲۱۹	۰/۱۶۱۷	۳۶۱/۴۸۵	۰/۱۴۴۷

Figure 7 demonstrates the variation of natural frequencies against the plate aspect ratio a/b. As the aspect ratio increases, a significant upward trend in the natural frequencies is observed. Physically, for a constant width b, an increase in a/b (meaning a longer plate in the a-direction) significantly alters the structural stiffness-to-mass ratio. In the context of the analyzed boundary conditions, higher aspect ratios lead to a more constrained geometric configuration relative to the vibration mode shapes, effectively increasing the geometric stiffness of the sandwich plate. Furthermore, the stiffening effect of the MR core (controlled by the magnetic field B) becomes more pronounced at higher aspect ratios, as the structural response becomes more sensitive to the shear modulus of the core layer.

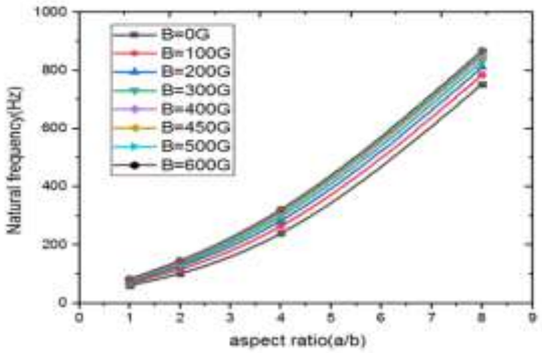

Figure 7. Influence of the plate aspect ratio a/b on the natural frequencies ω_n of the MR-cored sandwich plate under simply supported boundary conditions, evaluated across magnetic field intensities of B for $h_c/h_t = 1$.

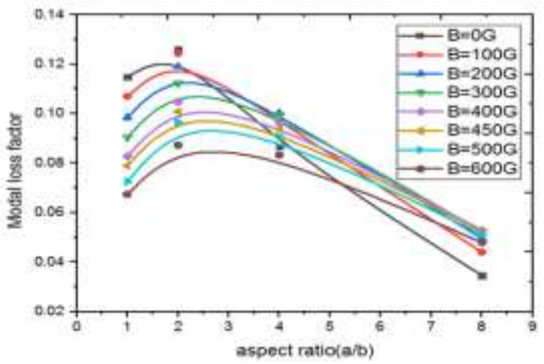

Figure 8. Influence of the plate aspect ratio a/b on the modal loss factor η_v of the MR-cored sandwich plate under simply supported boundary conditions, evaluated across magnetic field intensities of B for $h_c/h_t = 1$.

According to Figure 8, the modal loss factor of the sandwich plate first increases and then decreases as the aspect ratio increases up to 2. The reason for this is that the natural frequency associated with the first mode decreases significantly with increasing aspect ratio, and this sharp reduction in natural frequency leads to a corresponding reduction in the total strain energy of the structure in the first mode, which in turn produces a marked increase in the modal loss factor. With a further increase in the aspect ratio beyond approximately 2, the natural frequency and consequently the total strain energy of the structure continue to decrease in the first mode, and due to the reduction in the energy dissipated within the structure, the modal loss factor associated with this mode also decreases.

٤.٤. Effect of plate thickness on the natural frequency and modal loss factor

Simply supported square sandwich plates with MR core and cross-ply layers for the facings (0/90/0/ core/0/90/0) have been used to investigate the effect of the length-to-thickness ratio on the frequency.

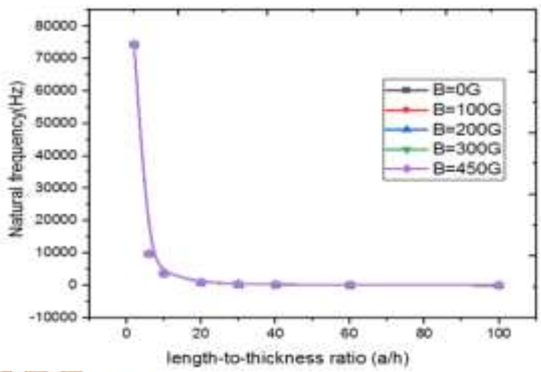

Figure 9. Influence of the length-to-thickness ratio a/h on the natural frequencies ω_n of the MR-cored sandwich plate under simply supported boundary conditions, evaluated across magnetic field intensities of B= 0, 100, 200, 300, and 450 Gauss, for h_c/h_t= 1 and a square plate geometry (a/b = 1).

Fig. 9 depicts the variation of natural frequencies as a function of the length-to-thickness ratio a/h. A sharp decline in the natural frequency is observed as the plate becomes thinner (increasing a/h. As the a/h ratio increases, the plate transitions from a 'thick plate' to a 'thin plate' regime, where the significant reduction in the flexural rigidity leads to a drastic decrease in the natural frequencies. Furthermore, at very high a/h ratios (thin plates), the effect of the magnetic field becomes less perceptible in the absolute frequency values, as the overall stiffness is dominated by the geometric slenderness of the structure.

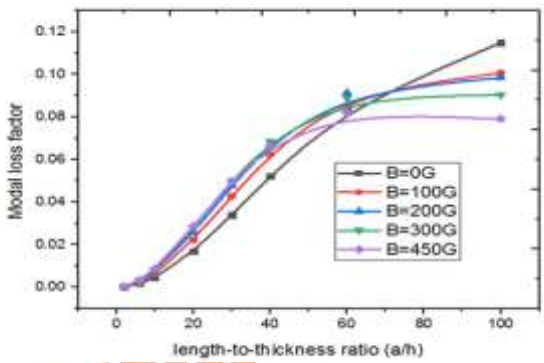

Figure 10. Influence of the length-to-thickness ratio a/h on the modal loss factor η_v of the MR-cored sandwich plate under simply supported boundary conditions, evaluated across magnetic field intensities of B= 0, 100, 200, 300, and 450 Gauss, for h_c/h_t= 1 and a square plate geometry (a/b = 1).

Fig. 10 illustrates the effect of the length-to-thickness ratio a/h on the modal loss factor. A compelling crossover behavior is observed: for thicker plates (lower a/h), higher magnetic fields enhance the loss factor, whereas for thinner plates (higher a/h), the trend reverses. Mechanically, this can be explained by the shift in the energy dissipation mechanism. In thin plates, the structural behavior is dominated by bending. As the magnetic field increases, the core becomes significantly stiffer, which can 'lock' the shear deformation or shift the strain energy toward the elastic face sheets. This reduction in the relative shear strain within the MR layer for very thin configurations leads to a decrease in the overall modal loss factor, despite the higher intrinsic damping capacity of the MR material at higher fields.

In this section, a dedicated discussion has been added to provide a rigorous physical justification of the observed trends in modal loss factor, grounded in the Modal Strain Energy (MSE) framework. It has been clarified that the overall modal loss factor $\boldsymbol{\eta_v}$ is not solely a function of the intrinsic material loss factor of the MR core, but is primarily governed by the fraction of the total strain energy stored in the dissipative core layer, expressed as:

$$\eta_v = \eta_{\text{core}} \times \frac{U_{\text{shear}}^{\text{MR}}}{U_{\text{total}}} = \frac{G''}{G'} \times \frac{U_{\text{shear}}^{\text{MR}}}{U_{\text{total}}}$$

where $U_{\text{shear}}^{\text{MR}}$ is the shear strain energy stored in the MR core, U_{total} is the total strain energy of the sandwich plate system, and $\eta_{\text{core}} = G''/G'$ is the intrinsic loss factor of the MR fluid, defined as the ratio of the loss modulus G'' to the storage modulus G' of the complex shear modulus $G = G' + iG''$.

The non-monotonic behavior of η_v observed in Figures 3, 5, and 10 is governed by the competition between two opposing mechanisms that respond differently to changes in the applied magnetic field intensity, core thickness ratio h_c/h_t, and length-to-thickness ratio a/h:

Mechanism 1 — Field-induced increase in intrinsic loss factor: At lower magnetic field intensities, G'' increases at a proportionally higher rate than G', causing $\eta_{\text{core}} = G''/G'$ to rise. Simultaneously, the stiffening of the MR core increases the shear strain energy fraction $U_{\text{shear}}^{\text{MR}}/U_{\text{total}}$, as a greater proportion of the total modal strain energy becomes concentrated in the core. Both effects act cooperatively in this regime, producing a progressive increase in η_v.

Mechanism 2 . Stiffening-induced reduction in energy fraction: As the magnetic field intensity increases further, the storage modulus G' begins to dominate over G'', reflecting the progressive development of the field-induced microstructure within the MR fluid. Although the core stiffens — which tends to increase $U_{\text{shear}}^{\text{MR}}/U_{\text{total}}$ the intrinsic loss factor $\eta_{\text{core}} = G''/G'$ simultaneously decreases as G' grows faster than G''. Beyond a critical field level, the reduction in η_{core} outweighs the gain in the energy fraction, and η_v begins to decline. This stiffening-dominated regime is responsible for the descending branch of the non-monotonic curves observed in the figures.

Equilibrium point Peak loss factor: The peaks observed in Figures 3, 5, and 10 represent the precise parametric conditions at which these two competing mechanisms reach equilibrium — that is, where the marginal gain in $U_{\text{shear}}^{\text{MR}}/U_{\text{total}}$ due to core stiffening is exactly offset by the marginal reduction in η_{core}. Beyond these peak points, the stiffening effect dominates and the modal loss factor declines, irrespective of the continued increase in the applied magnetic field, core thickness, or geometric slenderness ratio. These peak points therefore represent near-optimal operating conditions for the MR-cored sandwich plate in semi-active vibration control applications, and their identification across the parametric space of B, h_c/h_t, and a/h constitutes a key design insight of the present study.

5. Conclusions

In this study, a high-order vibration model for MR-cored composite sandwich plates was developed and validated. Beyond the numerical observations, the following fundamental conclusions regarding the structural physics of these systems can be drawn:

Dynamic Tunability: The research confirms that the MR core provides a robust mechanism for active vibration control. The natural frequencies can be shifted by changing the magnetic field, which is primarily due to the formation of particle chains within the MR elastomer, increasing the storage modulus

Optimal Damping Configuration: A critical finding is that the modal loss factor does not scale linearly with core thickness. The existence of an optimal core-to-panel thickness ratio $h_c/h \approx 0.7$ suggests that maximum energy dissipation occurs when there is a specific balance between the core's shear volume and the face sheets' bending constraint.

Stiffness-Damping Trade-off: The study identifies a "crossover" effect in damping performance related to plate slenderness. In thin plates, excessively high magnetic fields can "lock" the core's shear deformation, leading to a counter-intuitive reduction in the modal loss factor despite higher material damping.

Geometric Sensitivity: The sensitivity of the system to the aspect ratio a/b increases significantly at higher magnetic field intensities, indicating that the MR effect is more pronounced in geometrically constrained configurations.

The material parameters used in this simulation are selected to match the properties of standard MR fluids used in previous experimental studies [Ref]. Furthermore, the validity of the present modeling approach is ensured by the close agreement with the experimental results of Lall et al. [26] and RK Ojha [27], as presented in Table 1.

The current study relies on established empirical and analytical models to describe the behavior of MR-based structures. However, the integration of data-driven intelligence offers a significant opportunity to extend this framework. Specifically, the empirical MR models—which often involve nonlinearities that are difficult to capture analytically—could be replaced or enhanced by learned models based on neural networks (e.g., FCNNs or LSTMs), similar to the approaches demonstrated in recent literature [Dejanović et al., 2025]. Such an intelligent optimization framework could be utilized to automate the tuning of design parameters, such as magnetic field intensity and damping factors, leading to a more robust and adaptive vibration control system. This transition from traditional empirical modeling to machine learning-based estimation would not only reduce computational overhead but also increase the predictive accuracy in real-time engineering applications.

The primary novelty of this research lies in the development and rigorous implementation of a refined higher-order sinusoidal shear deformation theory for a thick sandwich panel with a Magnetorheological Core. Unlike previous studies that often rely on simplified first-order theories or conventional numerical approximations, this work provides a comprehensive symbolic-numerical framework developed in Wolfram Mathematica (version 12). This approach allows for:

1. The derivation of exact governing equations without the need for shear correction factors.
2. A more precise capture of the linear interaction between the MR core and the face layers.
3. The introduction of an optimized computational algorithm which enhances the accuracy of frequency response analysis compared to classical models.

These findings provide a practical design guideline for engineers to optimize the trade-off between structural weight, stiffness, and damping capacity in smart sandwich structures.

HIGHLIGHTS

To control the sandwich panel's natural linear vibration based on a New Sinusoidal shear deformation theory, the following facts were applied:

It shows that a magnetic field will change the stiffness of the sandwich rectangular plate. Thus, the natural frequencies and the modal loss factors are controllable when applying different intensities of magnetic fields.

The natural frequencies increase with increasing magnetic field for all the modes considered.

It was also noticed that there was an increase in the loss factors with increasing magnetic field for all the modes considered, except for a few modes.

It was shown that the natural frequency decreases with increasing thickness of the MR fluid layer for all the modes considered.

A significant variation in the natural frequencies was also observed for higher modes compared to those for lower modes.

It can be concluded that the amplitude of vibration could be considerably reduced using controllable MR fluids, and an MR fluid could be effectively used in controlling the vibrations of structures.

An increasing thickness of the MR core layer will also change the stiffness of the sandwich plate system. So, the natural frequency and modal loss factor can be controlled through a change in the thickness of the MR core layer.

6. References

1. Frostig, Y., Classical and high-order computational models in the analysis of modern sandwich panels. Composites Part B: Engineering, 2003. 34(1): p. 83–100.
2. Frostig, Y. and O.T. Thomsen, High-order free vibration of sandwich panels with a flexible core. International Journal of Solids and Structures, 2004. 41(5-6): p. 1697–1724.
3. Fard, K.M., M. Livani, and F.A. Ghasemi, Improved high-order free vibration analysis of thick double curved sandwich panels with transversely flexible cores. Latin American Journal of Solids and Structures, 2014. 11: p. 2284–2307.
4. Guerine, M.H.E., et al., On the free vibration behavior of carbon nanotube reinforced nanocomposite shells: a novel integral higher order shear theory approach. Structural Engineering and Mechanics, 2024. 91(1): p. 1–23.
5. Nayak, B., S. Dwivedy, and K. Murthy, Dynamic analysis of magnetorheological elastomer-based sandwich beam with conductive skins under various boundary conditions. Journal of Sound and Vibration, 2011. 330(9): p. 1837–1859.
6. Korobko, E.V., On damping vibrations of three-layered beam containing magnetorheological elastomer. Journal of Intelligent Material Systems and Structures, 2012. 23(9): p. 1019–1023.
7. Eshaghi, M., R. Sedaghati, and S. Rakheja, Dynamic characteristics and control of magnetorheological/electrorheological sandwich structures: a state-of-the-art review. Journal of Intelligent Material Systems and Structures, 2016. 27(15): p. 2003–2037.
8. Genç, S. and P.P. Phulé, Rheological properties of magnetorheological fluids. Smart Materials and Structures, 2002. 11(1): p. 140.
9. Slimani, O., et al., A new shear deformation shell theory for free vibration analysis of FG sandwich shells. Structural Engineering and Mechanics, An Int'l Journal, 2021. 78(6): p. 739–753.
10. Rajamohan, V., S. Rakheja, and R. Sedaghati, Vibration analysis of a partially treated multi-layer beam with magnetorheological fluid. Journal of Sound and Vibration, 2010. 329(17): p. 3451–3469.
11. Lara-Prieto, V., Vibration characteristics of MR cantilever sandwich beams: experimental study. Smart Materials and structures, 2009. 19(1): p. 015005.
12. Keshavarzian, M., Comparison of the application of smart electrorheological and magnetorheological fluid cores to damp sandwich panels' vibration behavior. Proceedings of the Institution of Mechanical Engineers, Part E: Journal of Process Mechanical Engineering, 2022. 236(2): p. 225–244.
13. Belabed, Z., et al., Shear-locking-free finite element formulation for vibrating functionally graded graphene nanocomposites using an enriched quadrilateral plate element. Engineering with Computers, 2025. 41(6): p. 4393–4415.

14. Widyatmoko, S., et al., A New Performing Quadrilateral Finite Element With 24 Degrees of Freedom Valid for Thin and Thick Shell Modelling: Formulation Aspects and Numerical Results. International Journal for Numerical Methods in Engineering, 2025. 126(24): p. e70207.
15. Manoharan, R., R. Vasudevan, and A. Jeevanantham, Dynamic characterization of a laminated composite magnetorheological fluid sandwich plate. Smart Materials and Structures, 2014. 23(2): p. 025022.
16. Yeh, J.-Y., Vibration analysis of sandwich rectangular plates with magnetorheological elastomer damping treatment. Smart Materials and Structures, 2013. 22(3): p. 035010.
17. Payganeh, G., K. Malekzadeh, and M.H. MALEK, Free vibration of sandwich panels with smart magneto-rheological layers and flexible cores. International Journal of Applied Mechanics, 2016.
18. Phuc, P.M. and V.N. Thanh, A new sinusoidal shear deformation theory for static bending analysis of functionally graded plates resting on Winkler–Pasternak foundations. Advances in Civil Engineering, 2021. 2021(1): p. 6645211.
19. Rezaiee-Pajand, M., M. Mokhtari, and A.R. Masoodi, Stability and free vibration analysis of tapered sandwich columns with functionally graded core and flexible connections. CEAS Aeronautical Journal, 2018. 9(4): p. 629–648.
20. Rezaiee-Pajand, M., E. Arabi, and A.R. Masoodi, Nonlinear analysis of FG-sandwich plates and shells. Aerospace Science and Technology, 2019. 87: p. 178–189.
21. Ghandehari, M.A., A.R. Masoodi, and S.E.S. Hosseininia, Multiscale dynamic behavior of imperfect hybrid matrix/fiber nanocomposite nested conical shells with elastic interlayer. Thin-Walled Structures, 2024. 205: p. 112494.
22. Dejanović, M., et al., Neural Network-Based Optimization of Repair Rate Estimation in Performance-Based Logistics Systems. Information, 2025. 16(12): p. 1031.
23. Phuc, P.M. and V.N. Thanh, A New Sinusoidal Shear Deformation Theory for Static Bending Analysis of Functionally Graded Plates Resting on Winkler–Pasternak Foundations. Advances in Civil Engineering, 2021. 2021.
24. Reddy, J.N., Mechanics of laminated composite plates and shells: theory and analysis. 2003: CRC press.
25. Mohammadi, N., An experimental evaluation of pre-yield and post-yield rheological models of magnetic field dependent smart materials. Journal of mechanical science and technology, 2010. 24: p. 1829–1837.
27. Rajamohan, V., R. Sedaghati, and S. Rakheja, Vibration analysis of a multi-layer beam containing magnetorheological fluid. Smart Materials and Structures, 2009. 19(1): p. 015013.
28. Lall, A., N. Asnani, and B. Nakra, Vibration and damping analysis of rectangular plate with partially covered constrained viscoelastic layer. Journal of Sound and Vibration, 1987.
29. Ojha, R. and S. Dwivedy, Dynamic analysis of sandwich plates with isotropic skins and viscoelastic core. International Journal of Structural Stability and Dynamics, 2019. 19(03): p. 1950033.